Forschungszentrum Karlsruhe
in der Helmholtz-Gemeinschaft

Wissenschaftliche Berichte
FZKA 6932

A Compact Introduction to the Numerical Modeling of Multiphase Flows

M. Wörner

Institut für Reaktorsicherheit
Programm Nukleare Sicherheitsforschung

November 2003

Forschungszentrum Karlsruhe
in der Helmholtz-Gemeinschaft

Wissenschaftliche Berichte

FZKA 6932

A compact introduction to the numerical modeling of multiphase flows

Martin Wörner

Institut für Reaktorsicherheit
Programm Nukleare Sicherheitsforschung

Forschungszentrum Karlsruhe GmbH, Karlsruhe
2003

Impressum der Print-Ausgabe:

Als Manuskript gedruckt

Forschungszentrum Karlsruhe GmbH
Postfach 3640, 76021 Karlsruhe

Mitglied der Hermann von Helmholtz-Gemeinschaft
Deutscher Forschungszentren (HGF)

ISSN 0947-8620

A compact introduction to the numerical modeling of multiphase flows

Abstract

This report represents the handouts of an eight hour lecture held on occasion of the "International Summer School on Computational Modeling of Combustion & Multiphase Flows in Energy Systems". This summer school took place in Neptun-Olimp, Romania, in the period of July 21 – 25, 2003.

The purpose of this report is to give students that are already familiar with the physics and numerical computation of single phase flow a compact introduction into the computational modeling of multiphase flows. The report is restricted to the hydrodynamics of multiphase flow and does not consider heat transfer, mass transfer and phase change. The report gives first an insight in the fundamental hydrodynamical phenomena of multiphase flows. It then presents the most popular modeling concepts for multiphase flows and points out their achievements and limitations. It details the continuous or interpenetrating field formulation of two-phase flow based on a volume averaging procedure and presents the related models as there are the homogeneous model, the diffusion model and drift flux model, and the two-fluid model. The report also discusses the Euler-Lagrange approach for disperse flow as well as interface resolving simulation methods such as the volume-of-fluid method, the level-set method and the front-tracking method.

Eine kompakte Einführung in die numerische Modellierung von Mehrphasenströmungen

Zusammenfassung

Der vorliegende Bericht stellt eine ergänzende schriftliche Unterlage zu einer acht Stunden umfassenden Vorlesung dar, die im Rahmen der "International Summer School on Computational Modeling of Combustion & Multiphase Flows in Energy Systems" gehalten wurde. Die Sommer-Schule fand vom 21.–25. Juli 2003 in Neptun-Olimp, Rumänien, statt.

Das Ziel dieses Berichtes ist es, Studenten, die bereits über Kenntnisse zur Physik und zur numerischen Berechnung einphasiger Strömungen verfügen, eine kompakte Einführung in die numerische Modellierung von Mehrphasenströmungen zu geben. Der Bericht beschränkt sich dabei auf die Hydrodynamik und behandelt nicht Wärmeübergang, Stoffübergang und Phasenübergang. Er gibt einen Überblick zu den grundlegenden hydrodynamischen Phänomenen in mehrphasigen Strömungen, stellt die am häufigsten verwendeten Modellierungskonzepte vor, und geht auf deren Errungenschaften und Einschränkungen ein. Das Konzept der Formulierung der Mehrphasenströmung als einander sich durchdringende Kontinua wird basierend auf einer Volumenmittelung hergeleitet. Als dazu in Beziehung stehende Modelle werden das homogene Modell, das Diffusions- und Drift-Strömungs-Modell und das Zwei-Fluid-Modell vorgestellt. Der Bericht behandelt weiter das Euler-Lagrange-Modell für disperse Strömung sowie Methoden zur detaillierten numerischen Beschreibung der Phasengrenzflächendynamik, wie die Volume-of-Fluid Methode, die Level-Set-Methode und die Front-Tracking-Methode.

Contents

Nomenclature

English

a_i	interfacial area concentration
$\mathcal{A}$	area
$\mathcal{A}_\mathrm{pcs}$	projected cross-sectional area of particle
C_am	added mass coefficient
C_D	drag coefficient
d	diameter
$\mathbb{D}_1, \mathbb{D}_2$	deformation tensor
$\mathbb{D}_\mathrm{i}$	momentum drift flux tensor
$\hat{\mathbf{e}}$	unit vector
Eo	Eötvös number
Eu	Euler number
f	liquid volumetric fraction
$\mathbf{f}$	force per unit volume
$\mathbf{F}$	force
g	acceleration of gravity
$\mathbf{g}$	gravity vector
H	mean curvature
$\mathbb{I}$	unit tensor
$\mathbf{j}$	superficial velocity
k	turbulent kinetic energy
m_p	particle mass
$\mathbf{M}_1, \mathbf{M}_2$	momentum transfer terms
Mo	Morton number
N_p	number of particles
n_p	particle number density
$\hat{\mathbf{n}}_1$, $\hat{\mathbf{n}}_2$	unit vector to the interface pointing in phase 1 and 2, respectively
p	pressure
R	radius
Re	Reynolds number
S_i	phase interface
St	Stokes number
t	time
$\mathbb{T}$	stress tensor
U	velocity of continuous phase
V	velocity of disperse phase, averaging volume
V_c	volume of mesh cell
$\mathbf{V}_\mathrm{p}$	translational velocity of center-of-mass of particle
$\mathcal{V}$	volume
$\mathbf{v}$	velocity field
We	Weber number
$\mathbf{x}$	position vector
X_k	phase indicator function
$\mathbf{X}_\mathrm{p}$	position vector to center-of-mass of particle

Greek

α_1, α_2	volume fraction
Γ_1, Γ_2	mass transfer across interface due to phase change
Γ_μ	viscosity ratio
Γ_ρ	density ratio
δ	Dirac delta function
ε	dissipation rate of turbulent kinetic energy
κ	interface curvature
μ	dynamic viscosity
ρ	density
$\Delta\rho$	absolute value of density difference
σ	coefficient of surface tension
τ_p	particle response time
ϕ	level-set function
ψ	sphericity
Ω	domain

Subscripts

1	phase 1 (continuous phase)
2	phase 2 (disperse phase)
B	bubble
body	body force
buoy	buoyancy
c	continuous
d	disperse
eq	equivalent
grav	gravity
h, hydr	hydrodynamic
i	interface
k	phase index ($k = 1, 2$)
m	mixture
p	particle
r	relative
surf	surface
turb	turbulent
T	terminal velocity

Superscripts

sgs	subgrid stress
T	transposed vector or tensor

Fonts

$\mathbf{f}, \mathbf{F}$	vector
f, F	scalar ($f = \lvert\mathbf{f}\rvert, F = \lvert\mathbf{f}\rvert$)
$\hat{\mathbf{f}}$	unit vector
$\mathbb{F}$	tensor

1 Introduction

The purpose of this lecture is to give an insight in the physics of multiphase flow, its mathematical description, and its physical modelling for numerical computation by computer codes. Both the physical modelling and the numerical computation of multiphase flows are associated with certain difficulties. Both kinds of difficulties mainly arise from the existence of moving interfaces separating the phases or immiscible fluids. In general, the geometry of the interfaces and the spatial distribution of the phases are not known a priori but are part of the solution. The difficulties in modelling concern the physical transfer processes taking place across the interface such as momentum, heat and mass transfer, and phase change. The numerical difficulties arise from the fact that the interface is moving and certain quantities are discontinuous across the interface, e.g. the density, viscosity, pressure.

This lecture does not aim to give a comprehensive overview neither on the subject of numerical methods for multiphase flows nor on the subject of physical models and respective closure assumptions. Instead, it aims to give an insight in the physical phenomena and to point out the specific assumptions involved in the most popular modelling concepts. This should allow the user of any computer code for computational fluid dynamics (CFD) to be aware of the achievements and limitations of available methods. Through this the user should be able to select the most appropriate physical model and numerical approach for any specific flow problem under consideration.

This lecture focuses especially on gas-liquid and liquid-liquid flows. Flows involving rigid particles are also considered, however, under the restriction of low volumetric concentration. Thus, fluidized beds are not discussed and the reader is referred to textbooks, e.g. [21]. Furthermore, the lecture is restricted to the hydrodynamics of multiphase flows. Thus, phenomena such as heat transfer, mass transfer, and phase change which are often associated with two-phase flows in engineering applications will not be discussed here. The interested reader is referred to textbooks, e.g. [5].

2 Fundamentals of multiphase flow

2.1 Notions

We start by giving a short description of several terms relevant to multiphase flows.

A *phase* is a thermodynamic definition for the state of matter, which can be either solid, liquid or gas. In a multiphase flow several phases flow together. These phases may consist of one chemical *component*, e.g. flow of water and water vapor (steam), or of several chemical components, e.g. flow of oil and water.

Within the general multiphase terminology a phase is classified as *continuous* if it occupies continuously connected regions of space and is classified as *disperse* when it occupies disconnected regions of space. The continuous phase may be gaseous or liquid. The disperse phase is formed by particles. In the sequel *particle* can mean either a rigid (solid) particle or a fluid particle. Fluid particles formed by a gas phase are denoted as bubbles, while fluid particles formed by a liquid phase are called drops. Throughout this paper we denote the continuous phase by subscript "c" and the disperse phase by subscript "d". Alternatively, we denote the phases by subscript k, where $k \in 1, 2$. Phase one ($k = 1$) is assumed to be continuous, while phase two ($k = 2$) can be continuous, too, or disperse.

In two-phase or multi-fluid flow the motion of all phases is of interest. It therefore differs from *free surface flows* in which the influence of the gas density and viscosity is neglected and only the motion within a liquid phase is of interest, as is the case e.g. for a stream of lava. In this lecture methods that are specially suited for free surface flows will not be considered.

2.2 Morphology and gas-liquid flow regimes in pipes

Gas-liquid two-phase flows can appear in quite different topological or morphological configurations. These different structures are usually called *flow regimes* or *flow patterns*. The special significance of the flow regime arises from the fact that the various physical transfer processes taking place across the phase-interface strongly depend on the flow regime. Therefore, the selection of adequate models for interfacial transport requires the identification of the flow regime first. Figure 1 and Figure 2 show flow regimes that typically occur in a horizontal and a vertical pipe, respectively.

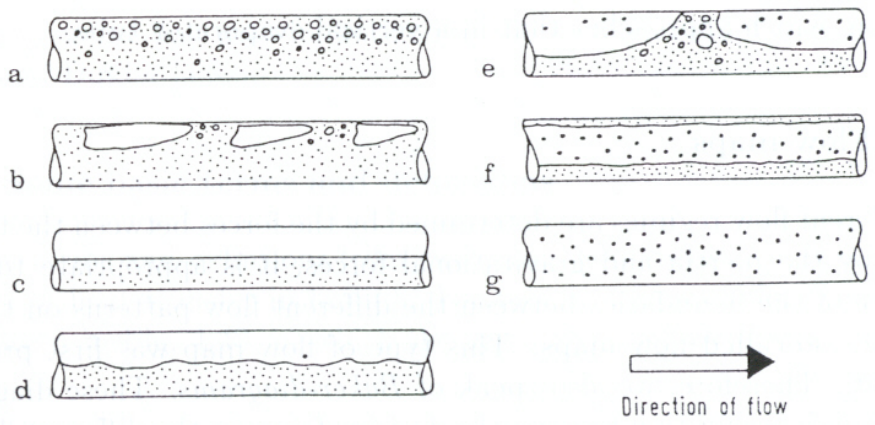

Fig. 4.45: Flow patterns in a horizontal, unheated tube **a** bubble flow; **b** plug flow; **c** stratified flow; **d** wavy flow; **e** slug flow; **f** annular flow; **g** spray or drop flow

Figure 1: Illustration of different flow regimes in a horizontal pipe (Figure from [5])

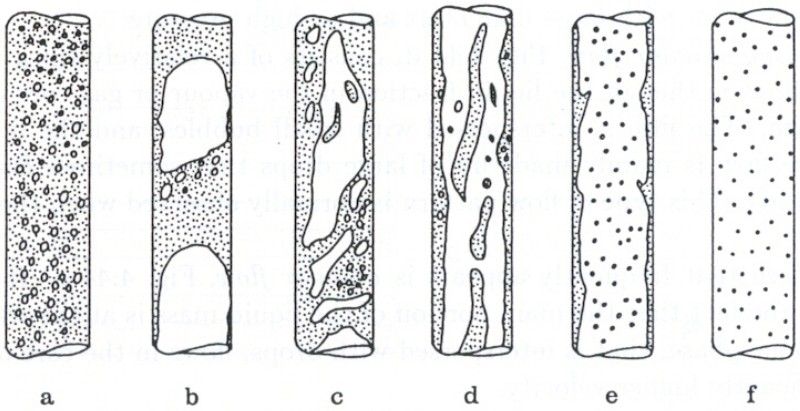

Fig. 4.44: Flow types in a vertical, unheated tube with upward flow. **a** Bubble flow; **b** Plug flow; **c** Churn flow; **d** Wispy-annular flow; **e** Annular flow; **f** Spray or drop flow

Figure 2: Illustration of different flow regimes in a vertical pipe (Figure from [5])

The conventional parameters used to identify flow regimes are the superficial velocities of the phases. These represent the volumetric flow rate of the respective phase divided by the channel cross-sectional area. However, the superficial velocities of the phases alone are usually

not sufficient to characterize the geometrical configuration of two-phase flows. In general, the flow regime depends on the physical properties of the phases or fluids and also on the channel geometry, e.g. the pipe diameter.

2.3 Fundamental forces in multiphase flow

Any fluid motion origins from forces acting on fluid elements. In general, forces can be classified in three different categories. *Volume forces* (also called body forces) act on a volume element of size $\mathcal{V} \propto L^3$, *surface forces* act on a surface or area element of size $\mathcal{A} \propto L^2$, and *line forces* act on a curve element of size $\mathcal{C} \propto L$, where L is a linear dimension. In Table 1 we summarize the forces that are important in two-phase flow.

The **pressure force** acts on area or surface elements and tends to accelerate the fluid in direction of the pressure gradient. The **inertia force** is a volume force and tends to retain the actual direction and magnitude of the motion unchanged. The **viscous force** acts on a surface or area element and tends to make the flow field uniform and thus to diminish velocity differences. The **gravity force** tends to accelerate the fluid in direction of the gravity vector. Related to the gravity force is the **buoyancy force**, which is the difference between the gravity force and the Archimedes force. The buoyancy force represents the net action of the gravity when the density is non-uniform. In single phase flows this density variation may be caused by temperature differences resulting in natural convection. In two-phase flow the non-uniform density is due to the presence of different phases. The **surface tension force** acts on a line or curve element and tends to minimize the surface area of the interface. The surface tension force is specific to gas-liquid or liquid-liquid two-phase flows.

Table 1: Forces in multiphase flows and their magnitude

		Magnitude of	
Force	type	force	force per unit volume
Pressure force	surface force	$F_\mathrm{P} \propto \mathcal{A}\Delta p$	$f_\mathrm{P} \propto \Delta p L^{-1}$
Inertia force	volume force	$F_\mathrm{I} \propto \mathcal{V}\rho U^2 L^{-1}$	$f_\mathrm{I} \propto \rho U^2 L^{-1}$
Viscous force	surface force	$F_\mathrm{V} \propto \mathcal{A}\mu U L^{-1}$	$f_\mathrm{V} \propto \mu U L^{-2}$
Gravity force	volume force	$F_\mathrm{G} \propto \mathcal{V} g\rho$	$f_\mathrm{G} \propto g\rho$
Buoyancy force	volume force	$F_\mathrm{B} \propto \mathcal{V} g\Delta\rho$	$f_\mathrm{B} \propto g\Delta\rho$
Surface tension force	line force	$F_\mathrm{S} \propto \mathcal{C}\sigma$	$f_\mathrm{S} \propto \sigma L^{-2}$

2.4 Non-dimensional groups

In technical two-phase flows the forces discussed above may be of quite different importance. Before one starts to attack a flow problem numerically it is useful to get an idea about the magnitude of the different forces involved. A proper way to identify the dominant forces and those forces that may be neglected is provided by dimensionless groups, expressing the ratio between two forces. From the six fundamental forces mentioned in Table 1 five independent non-dimensional groups can be derived. These groups often bear the name of important scientists. The probably best known non-dimensional group is the **Reynolds number**, representing the ratio between inertia and viscous forces:

$$Re = \frac{F_\mathrm{I}}{F_\mathrm{V}} = \frac{f_\mathrm{I}}{f_\mathrm{V}} = \frac{\rho L U}{\mu}$$

The **Euler number** represents the ratio between pressure gradient and inertia forces:

$$Eu = \frac{F_\mathrm{P}}{F_\mathrm{I}} = \frac{f_\mathrm{P}}{f_\mathrm{I}} = \frac{\Delta p}{\rho U^2}$$

The **Froude number** characterizes the ratio of inertia and gravity forces:

$$Fr = \frac{F_\mathrm{I}}{F_\mathrm{G}} = \frac{f_\mathrm{I}}{f_\mathrm{G}} = \frac{U^2}{gL}$$

Next we list non-dimensional groups that are specific to gas-liquid and liquid-liquid two-phase flows, because they involve the surface tension force. The **Weber number** represents the ratio of inertia forces to surface tension forces

$$We = \frac{F_\mathrm{I}}{F_\mathrm{S}} = \frac{f_\mathrm{I}}{f_\mathrm{S}} = \frac{\rho L U^2}{\sigma}$$

and the **Eötvös number** the ratio between buoyancy forces and surfaces tension forces

$$Eo = \frac{F_\mathrm{B}}{F_\mathrm{S}} = \frac{f_\mathrm{B}}{f_\mathrm{S}} = \frac{\Delta\rho g L^2}{\sigma}$$

From the above non-dimensional groups further groups can be defined. An example is the **Capillary number**

$$Ca = \frac{F_\mathrm{V}}{F_\mathrm{S}} = \frac{f_\mathrm{V}}{f_\mathrm{S}} = \frac{\mu U}{\sigma} = \frac{We}{Re}$$

which represents the ratio between viscous and surface tension forces. A particular useful number for gas-liquid and liquid-liquid flows is the **Morton number** which involves the continuous phase density and viscosity and is defined as

$$Mo = \frac{F_\mathrm{B} F_\mathrm{V}^4}{F_\mathrm{I}^2 F_\mathrm{S}^3} = \frac{g\Delta\rho\mu_c^4}{\rho_c^2\sigma^3} = \frac{EoWe^2}{Re^4} \tag{1}$$

The Morton number involves only fluid properties. Thus, for a given isothermal incompressible two-phase system it is a constant. For real fluids the Morton number ranges between 10^{-14} for gas bubbles in liquid metals and 10^8 for gas bubbles in viscous oils. For air bubbles in water the value of the Morton number is $Mo = 2.48 \cdot 10^{-11}$.

Two further non-dimensional groups are the density and viscosity ratio of the phases

$$\Gamma_\rho = \frac{\rho_d}{\rho_c}, \qquad \Gamma_\mu = \frac{\mu_d}{\mu_c}$$

Up to now, the characteristic length and velocity scales L and U appearing in the above dimensional groups have not been specified. A meaningful choice for these quantities depends on the type of flow under consideration. For the motion of rigid or fluid particles under the action of gravity, for example, a useful characteristic velocity scale is the terminal vertical velocity V_T of rise, respectively fall. A suitable length scale is the volume equivalent diameter d_eq. This is the diameter of a sphere that has the same volume $\mathcal{V}_\mathrm{p}$ as the particle

$$d_\mathrm{eq} \equiv \left(\frac{6\mathcal{V}_\mathrm{p}}{\pi}\right)^{\frac{1}{3}}$$

Similarly, a surface equivalent diameter can be defined

$$d_\mathrm{s} \equiv \left(\frac{\mathcal{A}_\mathrm{p}}{\pi}\right)^{\frac{1}{2}}$$

which is the diameter of a sphere that has the same surface area, $\mathcal{A}_\mathrm{p}$, as the particle. Another characteristic diameter that is commonly used is the Sauter diameter

$$d_{32} \equiv \frac{6\mathcal{V}_\mathrm{p}}{\mathcal{A}_\mathrm{p}}$$

For a sphere the above diameters are all equivalent and are equal to the diameter of the sphere.

The square of the ratio of equivalent diameter to surface diameter constitutes the **sphericity**

$$\psi = \frac{\text{surface area of volume-equivalent sphere}}{\text{surface area of particle}} = \frac{\pi d_\mathrm{eq}^2}{\pi d_\mathrm{s}^2} = \left(\frac{d_\mathrm{eq}}{d_\mathrm{s}}\right)^2 \tag{2}$$

wich represents a shape factor. As a spherical particle has the smallest possible area per unit volume the maximum value of the sphericity is 1. Thus, for any particle shape the values of the sphericity are in the range $0 < \psi \leq 1$.

2.5 The free rise of bubbles

There exists a large amount of research on the free rise or fall of isolated particles and particles in swarms or suspensions. By isolated we mean a single particle that is dispersed in a surrounding fluid of large extent. In section 2.5.1 we discuss the free rise of isolated bubbles in stagnant liquid. This is followed by a discussion on the effect of volumetric concentration on the rise or fall of a swarm or suspension of particles in section 2.5.2.

2.5.1 The free rise of an isolated bubble

Figure 3 shows experimental data for the terminal velocity, V_T, of air bubbles rising in water as function of equivalent diameter, respectively Eötvös number. Data are given for bubbles rising in a pure system (upper line) and in a "contaminated system" (lower line), while the region in between is shaded. Here contaminated means that the water may include small impurities or surface active substances often called "surfactants". The diagram in Figure 3 is classified in three main regimes. For small diameters the bubble is spherical and rises along a rectilinear path. For very large bubbles the rise is rectilinear too, while the bubble shape is spherical cap like. Both, in the spherical regime and the spherical-cap regime the rise velocity increases with equivalent diameter and the dependence of the rise velocity on the purity of the system is very week. For intermediate diameter the regime in Figure 3 is denoted as ellipsoidal. This regime is the most complex one and shows large scatter of the data, depending on the purity of the water. For contaminated water the rise velocity monotonically increases with diameter and the path is rectilinear. For pure water and in the ellipsoidal regime the rise velocity first increases with increasing bubble size. However, after a local maximum of the rise velocity is reached, the vertical velocity decreases until a local minimum and then increases again. If the equivalent diameter is smaller than the one corresponding to the local maximum in the rise velocity the shape of the ellipsoidal bubble is stable and the path is rectilinear. For diameters larger than that one corresponding to the local maximum of the rise velocity the bubble shape is still stable but wake instabilities induce a oscillatory instability of the bubble path. The path is then either zigzag or helical. This results in the decrease of the vertical component of the bubble velocity. With further increase of the equivalent diameter the bubble shape becomes finally unstable too, and there are irregular oscillations of both, the bubble shape ("wobbling") and the path.

The terminal bubble velocities shown in Figure 3 are for the air-water system. In general, the terminal rise velocity depends on the physical properties of the two phases. The influence of the fluid properties is best quantified by the Morton number defined in Eq. (1). Figure 4 represents a generalization of Fig. 3 for arbitrary two-phase systems. It shows a collection of

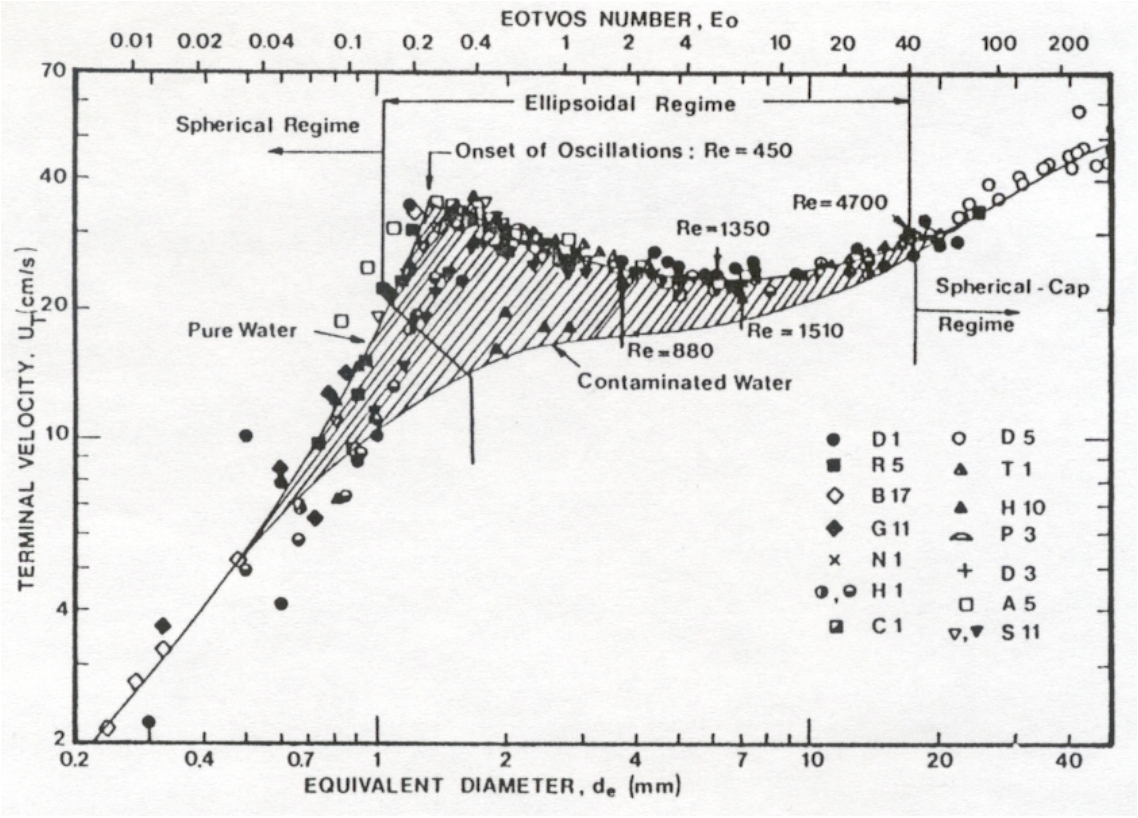

Figure 3: Terminal rise velocity of isolated air bubbles in water at 20℃ (Figure from [9])

experimental data for the bubble Reynolds number, $Re_{\mathrm{B}} \equiv \rho_c d_{\mathrm{eq}} V_{\mathrm{T}}/\mu_c$, as function of bubble Eötvös number, $Eo_{\mathrm{B}} \equiv \Delta\rho g d_{\mathrm{eq}}^2/\sigma$, and Morton number and also indicates regimes with different bubble shapes.

2.5.2 The rise of bubbles in a swarm

The concept of an isolated bubble is useful under the limit of vanishing volumetric concentration of the disperse phase. In practical applications particles are seldom isolated. Instead, the disperse phase has a finite volume fraction and, due to the presence of multiple particles, the particle-particle interaction becomes important. This is known to modify the velocity of rise or fall.

The influence of finite volumetric concentration is usually taken into account by an empirical relation originally proposed by Richardson & Zaki [27] for the suspension of mono-disperse rigid spheres

$$\frac{V_{\mathrm{susp}}}{V_{\mathrm{T}}} = (1 - \alpha_{\mathrm{p}})^{n-1} \tag{3}$$

Here, V_{T} is the terminal velocity of an isolated particle and V_{susp} is the velocity of a particle in a suspension of void fraction $\alpha_{\mathrm{p}} = \alpha_2$. For bubbles rising in a swarm there exist two regimes, namely hindered and cooperative rise regime. In the hindered rise regime, which is typically obtained with nearly spherical bubbles, the rise velocity in the swarm decreases with increasing gas volume fraction. In this case the exponent n is larger than unity. In contrast, with distorted bubbles there is a significant entrainment of bubbles in each others wake. The result of this "streaming" or "channeling" is an increase in the relative velocity with an increase of gas volumetric fraction. The exponent n in Eq. (3) therefore becomes less than unity.

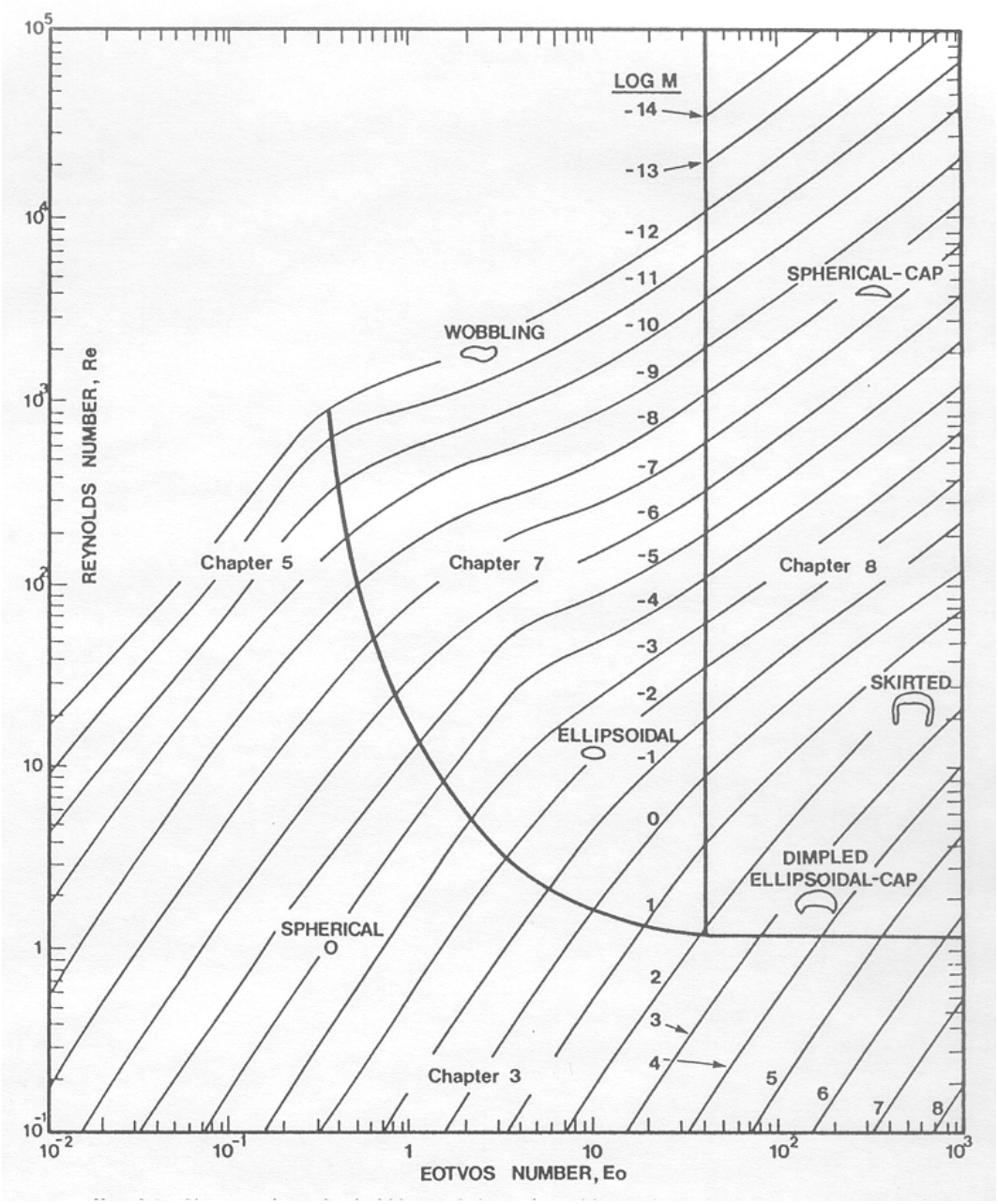

Figure 4: Bubble Reynolds number as function of bubble Eötvös number for different values of the Morton number (Figure from [9])

2.6 The forces on a particle immersed in a fluid

Consider a particle immersed in a continuous fluid. On each area element of the surface of the particle the surrounding fluid exerts a force. In Table 1 we identified two forces that act on surface elements, namely pressure forces and viscous forces. The resulting force exerted by the surrounding fluid on the particle is therefore given by the closed integral of the pressure and viscous stress distribution over the particles surface i.e. the phase interface.

In the sequel we consider only incompressible Newtonian fluids so that the following constitutive equation for the viscous stress applies

$$\mathbb{T}_k = 2\mu_k \mathbb{D}_k, \quad \text{where} \quad \mathbb{D}_k \equiv \frac{1}{2}\left(\nabla \mathbf{v}_k + (\nabla \mathbf{v}_k)^{\mathrm{T}}\right) \tag{4}$$

denotes the deformation tensor. We further assume that the viscosity μ_k is constant. The resulting force exerted by the fluid on the particles surface is then given by

$$\mathbf{F}_{\mathrm{surf}} = \oint_{\mathcal{A}_{\mathrm{p}}} (-p_1 \mathbb{I} + 2\mu_1 \mathbb{D}_1) \cdot \hat{\mathbf{n}}_1 \mathrm{d}S \tag{5}$$

Here, $\hat{\mathbf{n}}_1 = -\hat{\mathbf{n}}_2$ is the unit vector normal to the interface pointing into the continuous fluid (fluid 1) and $\mathbb{I}$ is the unit tensor.

To evaluate the integral in Eq. (5) it is useful to decompose the pressure p_1 in three contributions

$$p_1 = \rho_1 \mathbf{g} \cdot \mathbf{x} + P_{\mathrm{pg}} \hat{\mathbf{e}}_{\mathrm{p}} \cdot \mathbf{x} + p_{1,\mathrm{dyn}} \tag{6}$$

The first term on the r.h.s of Eq. (6) corresponds to the hydrostatic pressure, the second one to an external constant pressure gradient, and $p_{1,\mathrm{dyn}}$ denotes the dynamic pressure. Inserting Eq. (6) into Eq. (5) we obtain

$$\mathbf{F}_{\mathrm{surf}} = -\mathcal{V}_{\mathrm{p}} \left(\rho_1 \mathbf{g} + P_{\mathrm{pg}} \hat{\mathbf{e}}_{\mathrm{p}}\right) + \oint_{\mathcal{A}_{\mathrm{p}}} (-p_{1,\mathrm{dyn}} \mathbb{I} + 2\mu_1 \mathbb{D}_1) \cdot \hat{\mathbf{n}}_1 \mathrm{d}S = -\mathcal{V}_{\mathrm{p}} \left(\rho_1 \mathbf{g} + P_{\mathrm{pg}} \hat{\mathbf{e}}_{\mathrm{p}}\right) + \mathbf{F}_{\mathrm{hydr}} \tag{7}$$

Here, we used the Gauß divergence theorem to obtain

$$\oint_{\mathcal{A}_{\mathrm{p}}} (\rho_1 \mathbf{g} \cdot \mathbf{x} + P_{\mathrm{pg}} \hat{\mathbf{e}}_{\mathrm{p}} \cdot \mathbf{x}) \cdot \hat{\mathbf{n}}_1 \mathrm{d}S = \int_{\mathcal{V}_{\mathrm{p}}} \nabla \left(\rho_1 \mathbf{g} \cdot \mathbf{x} + P_{\mathrm{pg}} \hat{\mathbf{e}}_{\mathrm{p}} \cdot \mathbf{x}\right) \mathrm{d}V =$$

$$\int_{\mathcal{V}_{\mathrm{p}}} \left(\underbrace{\nabla \left(\rho_1 \mathbf{g} + P_{\mathrm{pg}} \hat{\mathbf{e}}_{\mathrm{p}}\right)}_{=0 \cdot \mathbb{I}} \cdot \mathbf{x} + \underbrace{\nabla \mathbf{x}}_{=\mathbb{I}} \cdot \left(\rho_1 \mathbf{g} + P_{\mathrm{pg}} \hat{\mathbf{e}}_{\mathrm{p}}\right) \right) \mathrm{d}V = \mathcal{V}_{\mathrm{p}} \left(\rho_1 \mathbf{g} + P_{\mathrm{pg}} \hat{\mathbf{e}}_{\mathrm{p}}\right)$$

From Eq. (7) we see that the resulting force exerted by the fluid on the particles surface consists of three contributions. The first one is due to the Archimedes force and the second one due to an external constant pressure drop. The third term represents the hydrodynamic force.

The hydrodynamic force $\mathbf{F}_{\mathrm{hydr}}$ can be split in a component $\mathbf{F}_{\mathrm{h}\parallel\mathrm{r}}$ with direction opposite to the relative velocity $\mathbf{U}_{\mathrm{r}}$ and in a component $\mathbf{F}_{\mathrm{h}\perp\mathrm{r}}$ normal to the relative velocity

$$\mathbf{F}_{\mathrm{hydr}} = \underbrace{\left(\mathbf{F}_{\mathrm{hydr}} \cdot \hat{\mathbf{e}}_{\mathrm{r}}\right)\left(-\hat{\mathbf{e}}_{\mathrm{r}}\right)}_{\mathbf{F}_{\mathrm{h}\parallel\mathrm{r}}} + \underbrace{\left[\mathbf{F}_{\mathrm{hydr}} - \left(\mathbf{F}_{\mathrm{hydr}} \cdot \hat{\mathbf{e}}_{\mathrm{r}}\right)\left(-\hat{\mathbf{e}}_{\mathrm{r}}\right)\right]}_{\mathbf{F}_{\mathrm{h}\perp\mathrm{r}}}, \quad \text{where} \quad \hat{\mathbf{e}}_{\mathrm{r}} = \frac{\mathbf{U}_{\mathrm{r}}}{|\mathbf{U}_{\mathrm{r}}|} = \frac{\mathbf{U}_{\mathrm{r}}}{U_{\mathrm{r}}}$$

is the unit vector in direction of the relative velocity.

The integral of the hydrodynamic force due to Eq. (7) can be computed analytically only for very special situations. One such situation is a rigid sphere (diameter d_{p}) moving in an otherwise motionless viscous fluid at very low Reynolds number (creeping flow). Stokes (1851)

was the first to determine the flow field and the resulting force when the sphere moves with constant velocity. His analysis was extended by Basset [6] to unsteady flow. The result is

$$\mathbf{F}_{\mathrm{hydr}} = \left\{ 3\pi\mu_1 d_\mathrm{p} V_\mathrm{p} + \frac{1}{2}\rho_1 \mathcal{V}_\mathrm{p} \frac{\mathrm{d}V_\mathrm{p}}{\mathrm{d}t} + \frac{3}{2}\sqrt{\pi\mu_1\rho_1}\, d_\mathrm{p}^2 \int_0^t \frac{\mathrm{d}V_\mathrm{p}(\tau)/\mathrm{d}\tau}{\sqrt{t-\tau}}\,\mathrm{d}\tau \right\} (-\hat{\mathbf{e}}_\mathrm{r}) \tag{8}$$

where $V_\mathrm{p}(t)$ is the instantaneous velocity of the sphere. It can be seen that in the case when the sphere moves steadily so that V_p is constant, the second and third term drop from the r.h.s of Eq. (8) and only the first term remains. This term represents the **Stokes drag force**. The second term on the r.h.s of Eq. (8) is denoted as **added mass force**. It represents the force required to accelerate the fluid surrounding the particle. The added mass force bears its name from the observation that particles resist accelerations stronger than is apparent from their actual mass. The added mass is also called virtual mass. The third term on the r.h.s of Eq. (8) is the **Basset force**. It describes the force due to the lagging boundary layer development with changing velocity. Because this force depends on the acceleration history up to the present time, the Basset force is also called history force.

From Eq. (8) it can be seen that for this special case the force component $\mathbf{F}_{\mathrm{h}\perp\mathrm{r}}$ is zero. We mention two situations where the transversal force component $\mathbf{F}_{\mathrm{h}\perp\mathrm{r}}$ is non-zero. The **Magnus force** is related to transversal forces acting on a rotating body. Placed in a *uniform flow field*, the particle rotation results in an increase in the velocity on one side and a decrease on the other side. This gives an asymmetrical pressure distribution around the particle. Particles in a *non-uniform flow field* such as a shear-flow exhibit similar lateral motion (without necessary rotation) as caused by the Magnus force for rotating particles in uniform flow. This force is called **Saffman force** [28, 29]. If the particle can freely move then the force component $\mathbf{F}_{\mathrm{h}\perp\mathrm{r}}$ results in a lateral movement of the particle. Therefore, all contributions to the force $\mathbf{F}_{\mathrm{h}\perp\mathrm{r}}$ are commonly denoted as **transversal lift force** or shortly as lift force.

In the most general case, when a rigid or fluid particle of arbitrary shape moves with time-dependent velocity in a possibly non-uniform flow field, the force $\mathbf{F}_{\mathrm{hydr}}$ cannot be determined analytically. Nevertheless, for this general case the structure of Eq. (8) is retained and the hydrodynamic force is split in several components

$$\mathbf{F}_{\mathrm{hydr}} = \mathbf{F}_{\mathrm{drag}} + \mathbf{F}_{\mathrm{am}} + \mathbf{F}_{\mathrm{hist}} + \mathbf{F}_{\mathrm{lift}} \tag{9}$$

which need to be determined from experiments. In this general case the relative velocity $\mathbf{U}_\mathrm{r}$ is expressed as

$$\mathbf{U}_\mathrm{r} = \mathbf{V}_\mathrm{p} - \mathbf{U}_\mathrm{c} \tag{10}$$

where $\mathbf{V}_\mathrm{p}$ is the translational velocity of the particle and $\mathbf{U}_\mathrm{c}$ is a characteristic velocity of the continuous phase. As will be seen below, the choice for $\mathbf{U}_\mathrm{c}$ depends on the specific modelling approach.

2.7 The drag force

The most important one of the four forces on the right hand side of Eq. (9) is the drag force. In this section we therefore summarize important analytical and experimental results related to the drag force.

2.7.1 Drag coefficient for an isolated rigid sphere

The drag force always acts opposite to the relative velocity of the particle. It represents a resistance the particle experiences due to the presence of the continuous phase. Equation (5) shows that both the pressure field and the viscous stresses contribute to the drag force. These

contributions are denoted as *form drag* and *friction drag* (viscous drag), respectively. The common concept to quantify the drag force is to define a non-dimensional **drag coefficient**

$$C_{\mathrm{D}} \equiv \frac{|\mathbf{F}_{\mathrm{drag}}|}{\frac{1}{2}\rho_1 \mathcal{A}_{\mathrm{pcs}} U_{\mathrm{r}}^2} \tag{11}$$

so that the drag force is given by

$$\mathbf{F}_{\mathrm{drag}} \equiv -\frac{1}{2}\rho_1 \mathcal{A}_{\mathrm{pcs}} C_{\mathrm{D}} |\mathbf{U}_{\mathrm{r}}| \mathbf{U}_{\mathrm{r}} \tag{12}$$

Here, $\mathcal{A}_{\mathrm{pcs}}$ is the projected cross sectional area of the particle normal to $\hat{\mathbf{e}}_{\mathrm{r}}$. The drag coefficient is a function of the particle Reynolds number. This is the Reynolds number based on the volume-equivalent diameter d_{eq} of the particle and on the magnitude of the relative velocity

$$Re_{\mathrm{p}} \equiv \frac{\rho_1 d_{\mathrm{eq}} U_{\mathrm{r}}}{\mu_1} \tag{13}$$

Furthermore, C_{D} is a function of the particle shape and orientation.

The drag force can be determined analytically only for special cases. For a single rigid spherical particle moving in an infinite fluid at low Reynolds number, say $Re_{\mathrm{p}} \leq 0.2$ (creeping flow), the insertion of the Stokes drag force (first term in Eq. (8)) in the definition of the drag coefficient, Eq. (11), results in the **Stokes drag law**

$$C_{\mathrm{D,St}} = \frac{24}{Re_{\mathrm{p}}} \tag{14}$$

In the Stokes regime (or viscous regime) the viscous drag is two times the form drag. For particle Reynolds numbers higher than unity the drag coefficient must be determined from experiments. With increasing Reynolds number the contribution of the form drag becomes more important and finally dominates over the viscous drag. In the range $750 < Re_{\mathrm{p}} < 3{\cdot}10^5$ the drag coefficient approaches a nearly constant value of $C_{\mathrm{D}} \approx 0.44$, see Figure 5. This is known as **inertial regime** or Newton's regime. With further increase of the Reynolds number there is a sudden decrease of the drag coefficient at the critical Reynolds number ($Re_{\mathrm{p}} \approx 3{\cdot}10^5$). This is because the boundary layer becomes turbulent and the separation point is moved rearwards, sharply reducing the form drag [8].

A reasonably good approximation for the drag coefficient of spherical particles in the transitional region between the Stokes and inertial regime, $0.2 < Re_{\mathrm{p}} < 1000$, is the correlation of Schiller and Naumann

$$C_{\mathrm{D,SN}} = \frac{24}{Re_{\mathrm{p}}}\left(1 + 0.15 Re_{\mathrm{p}}^{0.687}\right) \tag{15}$$

2.7.2 Drag coefficient for an isolated bubble or drop

An extension of Stokes' analysis to a *spherical fluid particle* is given by the Hadamard-Rybczynski drag law. For bubbles or drops the shear stress on the surface induces an internal motion. This results in a decrease of the drag coefficient

$$C_{\mathrm{D,HR}} = \frac{24}{Re_{\mathrm{p}}}\left(\frac{\frac{2}{3} + \Gamma_\mu}{1 + \Gamma_\mu}\right) = \left(\frac{\frac{2}{3} + \Gamma_\mu}{1 + \Gamma_\mu}\right) C_{\mathrm{D,St}} \tag{16}$$

Here, $\Gamma_\mu \equiv \mu_{\mathrm{d}}/\mu_{\mathrm{c}}$ is the viscosity ratio. For a droplet in air we have approximately $\Gamma_\mu \to \infty$ and the Stokes law is recovered. For a bubble in a liquid we have approximately $\Gamma_\mu \to 0$ so that the drag coefficient is reduced by one third and becomes $16/Re_{\mathrm{p}}$. While this analytical result of

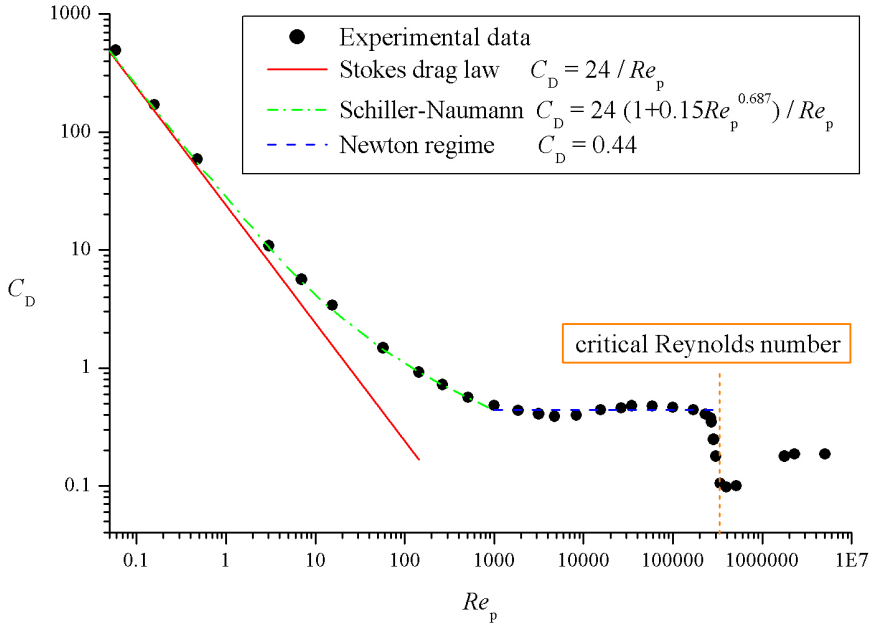

Figure 5: Drag curve for an isolated rigid sphere.

Hadamard and Rybczynski is valid for a spherical bubble at very low Reynolds number, Levich [24] derived analytically the drag coefficient for a spherical bubble at very high Reynolds number and obtained

$$C_{\mathrm{D,Lev}} = \frac{48}{Re_{\mathrm{p}}} \tag{17}$$

The analyses of Hadamard-Rybczynski and Levich are valid for a contaminant-free interface. In practice, until special care is taken, fluids always contain a small amount of surfactants that result in a slight contamination of the interface. This is supported from the empirical drag curve for an isolated air bubble in water and a drop of water in air as displayed in Figure 6. It can be seen that for Reynolds numbers below say 20 the drag of the bubble or drop does not differ from that of the rigid sphere, i.e. the curve which is in Figure 6 denoted as "standard drag curve". For particle Reynolds numbers larger than 20 the drag curves for a bubble in pure water and in contaminated water, however, clearly differ. For contaminated water the drag coefficient is always larger than the standard drag curve. In contrast, the drag of a bubble in pure water is smaller than that of a rigid sphere for $20 < Re_{\mathrm{p}} < 700$. This is an effect of the bubbles internal circulatory motion. For larger values of the Reynolds number the drag of the bubble exceeds that of the sphere having the same volume. This is due to the deformation of the bubble, resulting in an oblate ellipsoidal shape and thus causes a higher form drag as compared to a sphere. For values $Re_{\mathrm{p}} > 7,000$ the drag curve of an air bubble in pure and contaminated water match again, which is consistent with Figure 3, and C_{D} takes a value of about 8/3=2.67. This constant value of C_{D} for very large Reynolds number is in contrast to the result of Levich, Eq. (17), from which it follows that $C_{\mathrm{D}} \to 0$ for $Re_{\mathrm{p}} \to \infty$. However, the Levich drag coefficient is derived under the assumption of a spherical bubble while in reality at very large bubble Reynolds number the bubble shape is not spherical but of spherical cap type.

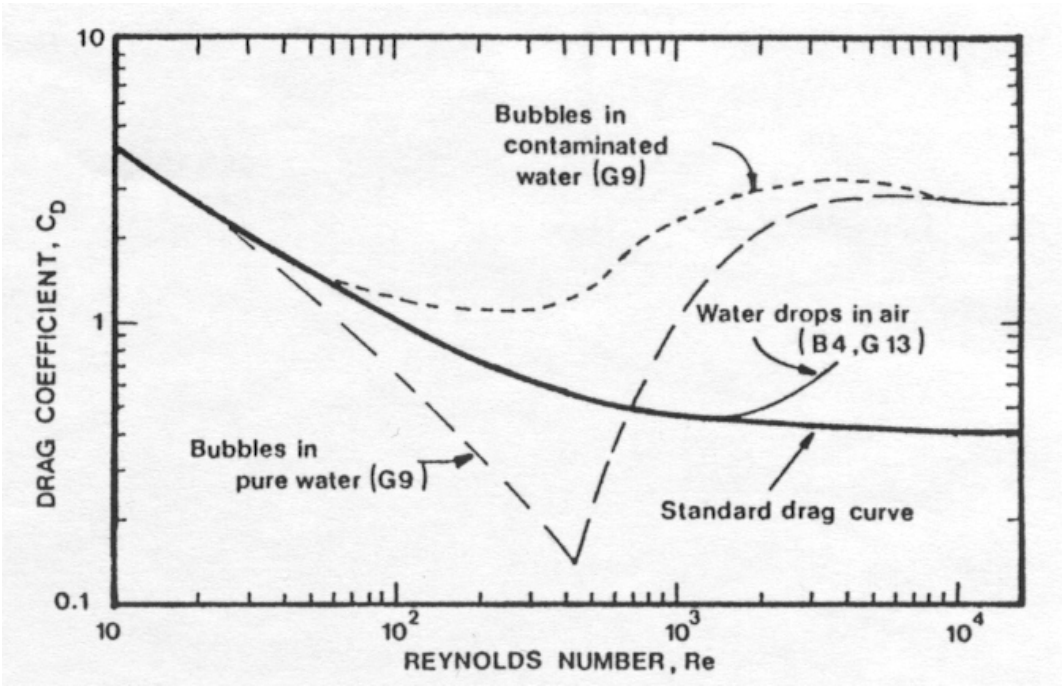

Figure 6: Drag curve for an isolated air bubble in pure and contaminated water and a water drop in air (Figure from [9]). For comparison the "standard drag curve" of a rigid sphere is also displayed.

2.7.3 Equilibrium between gravity, buoyancy, and drag force

We consider now the special case when a rigid particle, droplet or bubble of arbitrary shape sinks or rises with constant terminal velocity V_T within a stagnant fluid. Then the drag force is in balance with the gravity and buoyancy force and we have

$$|\mathbf{F}_{\mathrm{h}\|\mathrm{r}}| = |\mathbf{F}_{\mathrm{drag}}| = |\mathbf{F}_{\mathrm{grav}} + \mathbf{F}_{\mathrm{buoy}}| = \mathcal{V}_\mathrm{p} g|\rho_d - \rho_c| = \frac{\pi}{6} d_\mathrm{eq}^3 g \Delta\rho \tag{18}$$

Taking $\mathcal{A}_\mathrm{pcs} \approx \pi d_\mathrm{eq}^2/4$ and inserting Eq. (11) into Eq. (18) we obtain a relation between C_D and further non-dimensional groups

$$C_\mathrm{D} = \frac{4}{3}\frac{d_\mathrm{eq} g \Delta\rho}{\rho_\mathrm{c} V_\mathrm{T}^2} = \frac{4}{3}\frac{\Delta\rho}{\rho_\mathrm{c}}\frac{1}{Fr} = \frac{4}{3}\frac{Eo}{We} = \frac{4}{3} Mo \frac{Re^4}{We^3} = \frac{4}{3}\sqrt{\frac{Eo^3}{MoRe^4}}$$

2.8 Boundary conditions at a fluid interface

The boundary separating the bulk regions of two fluids is commonly denoted as interface. The interface is a material region across which physical quantities vary continuously. Under most situations the interface is only a few molecules thick. As this thickness is much smaller than other length scales of interest it is a useful practical concept to consider a "functional interface". While the thickness of the functional interface is zero it is associated with an interfacial tension σ. A finite thickness of the interface may, however, be of importance for moving contact lines and supercritical fluids. We refer to [2] for a review on diffuse interface methods that consider the interface thickness to be finite. In this paper we restrict our discussion on functional interfaces so that they can be viewed as discontinuities in the density and viscosity field.

At a functional interface the phases are coupled by a kinematic condition and a dynamic condition. For simplicity we assume throughout this lecture that no interfacial molecular diffusion (mass transfer) or phase change takes place. Then the **kinematic condition** states that

the velocity normal to the interface is continuous

$$\mathbf{v}_{1\mathrm{i}} \cdot \hat{\mathbf{n}}_1 = \mathbf{v}_{2\mathrm{i}} \cdot \hat{\mathbf{n}}_1 \tag{19}$$

If both fluids are viscous then also the tangential velocity at the interface is continuous so that

$$\mathbf{v}_{1\mathrm{i}} = \mathbf{v}_{2\mathrm{i}}$$

The **dynamic condition** states that at the interface the pressure and viscous stresses are in equilibrium with forces due to surface tension

$$-\left(p_{1\mathrm{i}} - p_{2\mathrm{i}}\right)\hat{\mathbf{n}}_1 + \left(\mathbb{T}_{1\mathrm{i}} - \mathbb{T}_{2\mathrm{i}}\right) \cdot \hat{\mathbf{n}}_1 = 2H\sigma\hat{\mathbf{n}}_1 + \nabla_{\mathrm{s}}\sigma \tag{20}$$

Here, $\nabla_{\mathrm{s}} \equiv \mathbb{I}_{\mathrm{s}} \cdot \nabla = (\mathbb{I} - \hat{\mathbf{n}}_1\hat{\mathbf{n}}_1) \cdot \nabla$ is the surface gradient operator. Insertion of Eq. (4) in Eq. (20) and projection in direction of the unit normal vector $\hat{\mathbf{n}}_1$ gives

$$-\left(p_{1\mathrm{i}} - p_{2\mathrm{i}}\right) + \left[\mu_1\left(\nabla\mathbf{v}_1 + (\nabla\mathbf{v}_1)^{\mathrm{T}}\right) - \mu_2\left(\nabla\mathbf{v}_2 + (\nabla\mathbf{v}_2)^{\mathrm{T}}\right)\right]_{\mathrm{i}} : \hat{\mathbf{n}}_1\hat{\mathbf{n}}_1 = 2H\sigma \tag{21}$$

while projection in the direction of a unit tangential vector $\hat{\mathbf{t}}$ gives

$$\left[\mu_1\left(\nabla\mathbf{v}_1 + (\nabla\mathbf{v}_1)^{\mathrm{T}}\right) - \mu_2\left(\nabla\mathbf{v}_2 + (\nabla\mathbf{v}_2)^{\mathrm{T}}\right)\right]_{\mathrm{i}} : \hat{\mathbf{n}}_1\hat{\mathbf{t}} = (\nabla_{\mathrm{s}}\sigma) \cdot \hat{\mathbf{t}} \tag{22}$$

Here, H is the mean curvature

$$H \equiv \frac{1}{2}\left(\frac{1}{R_{\min}} + \frac{1}{R_{\max}}\right) = -\frac{1}{2}\nabla_{\mathrm{s}}\hat{\mathbf{n}}_1 \tag{23}$$

and $R_{\min}$ and $R_{\max}$ are the principal radii of curvature. For constant surface tension and in the absence of gravity and any motion the fluid particle has a spherical shape and Eq. (21) reduces to the well known **Young-Laplace equation**

$$p_2 - p_1 = \frac{2\sigma}{R}$$

where R is the radius of the spherical bubble or drop.

In general, the coefficient of surface tension is not constant over the interface. There are two main reasons for a variation of σ, namely due to a non-uniformity of either temperature or the concentration of an absorbed material at the interface. From Eq. (22) it is evident that the resulting tangential force can be balanced only by a non-zero tangential viscous stress. Thus, a non-uniform coefficient of surface tension always induces some motion because it is impossible to fulfill Eq. (22) by fluids at rest.

In a free surface flow the viscosity of phase 2 is neglected. When the coefficient of surface tension is uniform, this results in a conditions of zero-tangential stress. If surface tension is neglected at all and so is the density of the gas phase, the dynamic boundary condition on the gas side of the interface is simply that of constant pressure p_2.

The neglect of the gas viscosity and density can also be a reasonable simplification for bubbles rising through liquid. Then, the zero-tangential stress boundary condition of a deformable bubble differs considerably from that of a non-deformable rigid particle for which the no-slip condition holds. These differences between bubbles and rigid particles influence the vorticity production at the surface and thereby the structure of the wakes and the forces exerted by the surrounding fluid.

3 Continuous field formulation of multiphase flow

In the remainder of this paper we present different methods for the numerical modelling of two-phase flows. In this section we discuss methods that are based on a continuum description of all the phases. The continuum approach can be applied to liquid, gaseous and rigid phases and relies on an averaging procedure. In literature, several types of averaging are used. These include time averaging [15], volume averaging [39] and ensemble averaging [10]. The latter represents the most general averaging procedure. All the averaging procedures yield averaged equations which formally have the same structure. Here, we restrict ourself to the volume averaging procedure.

We start this chapter by giving some mathematical prerequisites in section 3.1. In section 3.2 we present the derivation of volume averaged conservation equations. The set of equations obtained is not closed and therefore model assumptions must be introduced. Two-phase flows usually involve some relative motion of one phase with respect to the other. Within the continuous field approach, there are three main modelling concepts to describe this relative motion. These concepts differ in their complexity and therefore have different ranges of applicability. We introduce these models in increasing order of complexity and discuss in section 3.4 the homogeneous model, in section 3.5 the diffusion model and the closely related drift-flux model, and in section 3.6 the two-fluid model.

3.1 Mathematical prerequisites

3.1.1 Phase indicator function X_k

We consider two fluids or phases which occupy disjoint time-dependent domains $\Omega_k(t), k = 1, 2$ such that $\Omega = \Omega_1(t) \cup \Omega_2(t)$ is constant in time. We denote the boundaries of the respective domains by $\partial\Omega_1, \partial\Omega_2$ and $\partial\Omega$. The interface separating the fluids is then given by

$$S_\mathrm{i}(t) = (\partial\Omega_1 \cup \partial\Omega_2) \,/\, \partial\Omega$$

We now define for each phase a *phase indicator function* or *characteristic function* $X_k(\mathbf{x}, t)$ which is unity if the position vector $\mathbf{x}$ is in fluid k at time t and is zero otherwise

$$X_k(\mathbf{x}, t) = \begin{cases} 1, & \text{if } \mathbf{x} \in \Omega_k(t) \\ 0, & \text{otherwise} \end{cases}$$

The two phase indicator functions are related through the condition

$$X_1 + X_2 = 1 \tag{24}$$

The gradient of the phase indicator function is connected to the interface unit normal vector $\hat{\mathbf{n}}_k$ and the Dirac delta function of the interface $\delta(\mathbf{x} - \mathbf{x}_\mathrm{i}, t)$ by relation

$$\nabla X_k = \hat{\mathbf{n}}_k \delta(\mathbf{x} - \mathbf{x}_\mathrm{i}, t) \tag{25}$$

where $\mathbf{x}_\mathrm{i}$ is a point on the interface. Another important relation is the *topological equation*

$$\frac{\partial X_k}{\partial t} + \mathbf{v}_\mathrm{i} \cdot \nabla X_k = 0 \tag{26}$$

which expresses the fact that the material derivative of X_k is zero [10].

3.1.2 Volume averaging operators

We now introduce the method of volume averaging [10, 39]. For this purpose we consider a general representative volume element V which is bounded by the surface ∂V and is invariant with respect to time and space. The centroid of V is located at $\mathbf{x}$ and we use the relative position vector $\boldsymbol{\eta}$ to locate any point in V relative to the centroid so that $\mathbf{x}_\eta = \mathbf{x} + \boldsymbol{\eta}$. Then we obtain the volume fraction of phase k within volume element V as

$$\alpha_k \equiv \frac{1}{V}\int_V X_k(\mathbf{x}+\boldsymbol{\eta},t)\mathrm{d}\mathbf{x}_\eta = \frac{V_k}{V}$$

Next we define two volume averaging operators for a general scalar or vector quantity, ψ_k, over the entire volume element V and over the volume, V_k, occupied solely by phase k, respectively:

$$\overline{\psi_k}^V \equiv \frac{1}{V}\int_V \psi_k(\mathbf{x}+\boldsymbol{\eta},t)X_k(\mathbf{x}+\boldsymbol{\eta},t)\mathrm{d}\mathbf{x}_\eta$$

$$\overline{\psi_k}^k \equiv \frac{1}{V_k}\int_V \psi_k(\mathbf{x}+\boldsymbol{\eta},t)X_k(\mathbf{x}+\boldsymbol{\eta},t)\mathrm{d}\mathbf{x}_\eta$$

For each phase these averages are linearly related to one another through the respective volume fraction, namely

$$\overline{\psi_k}^V = \alpha_k \overline{\psi_k}^k$$

3.1.3 Gauß and Leibniz rule

To prepare the derivations of volume averaged equations to be presented in section 3.2 we first introduce two important rules for volume averaging. The **Gauß rule** for volume averaging reads [10]

$$\overline{X_k\nabla\psi_k}^V = \nabla\overline{X_k\psi_k}^V - \overline{\psi_k\nabla X_k}^V = \nabla\overline{X_k\psi_k}^V - \frac{1}{V}\int_{S_\mathrm{i}\cap V}\hat{\mathbf{n}}_k\psi_{k\mathrm{i}}(\mathbf{x}+\boldsymbol{\eta},t)\mathrm{d}S \tag{27}$$

Here, ψ_k is a general scalar or vector quantity and $\psi_{k\mathrm{i}}$ is the value of this quantity on the k-side of the interface. Furthermore, $S_\mathrm{i}\cap V$ denotes the part of the interface that is within the averaging volume V.

Similar to Eq. (27), one obtains for averages involving time derivatives the result

$$\overline{X_k\frac{\partial\psi_k}{\partial t}}^V = \frac{\partial}{\partial t}\overline{X_k\psi_k}^V - \overline{\psi_k\frac{\partial X_k}{\partial t}}^V$$

Using the topological equation (26) to replace $\partial X_k/\partial t$ we obtain the **Leibniz rule** for volume averaging [10]

$$\overline{X_k\frac{\partial\psi_k}{\partial t}}^V = \frac{\partial}{\partial t}\overline{X_k\psi_k}^V + \overline{\psi_k\mathbf{v}_\mathrm{i}\cdot\nabla X_k}^V = \frac{\partial}{\partial t}\overline{X_k\psi_k}^V + \frac{1}{V}\int_{S_\mathrm{i}\cap V}\hat{\mathbf{n}}_k\cdot\mathbf{v}_\mathrm{i}\psi_{k\mathrm{i}}(\mathbf{x}+\boldsymbol{\eta},t)\mathrm{d}S$$

3.2 Volume averaged equations

In this section we summarize the derivation of the volume averaged equations for a two-fluid system. For simplicity, we restrict our analysis to isothermal incompressible fluids only, so that the densities ρ_1 and ρ_2 will henceforth be assumed constant. The fluids flow with velocities $\mathbf{v}_1(\mathbf{x},t)$ and $\mathbf{v}_2(\mathbf{x},t)$. The local conservation equations for mass and momentum valid in $\Omega_k(t)$ are

$$\frac{\partial\rho_k}{\partial t} + \nabla\cdot\rho_k\mathbf{v}_k = 0 \tag{28}$$

and

$$\frac{\partial\left(\rho_k \mathbf{v}_k\right)}{\partial t} + \nabla \cdot \rho_k \mathbf{v}_k \mathbf{v}_k = -\nabla p_k + \rho_k \mathbf{g} + \nabla \cdot \mathbb{T}_k \tag{29}$$

respectively, where $k \in 1, 2$ and the viscous stress tensor $\mathbb{T}_k$ is given by Eq. (4).

3.2.1 Volume averaged equations for individual phases

Multiplying each of the equations (28) and (29) by the respective phase indicator function X_k and performing the average over V we obtain

$$\frac{\partial\left(\alpha_k \rho_k\right)}{\partial t} + \nabla \cdot \alpha_k \rho_k \overline{\mathbf{v}_k}^k = \Gamma_k \tag{30}$$

$$\frac{\partial\left(\alpha_k \rho_k \overline{\mathbf{v}_k}^k\right)}{\partial t} + \nabla \cdot \alpha_k \rho_k \overline{\mathbf{v}_k \mathbf{v}_k}^k = -\nabla\left(\alpha_k \overline{p_k}^k\right) + \alpha_k \rho_k \mathbf{g} + \nabla \cdot \alpha_k \overline{\mathbb{T}_k}^k + \mathbf{M}_k \tag{31}$$

The terms Γ_k and $\mathbf{M}_k$ are due to the Gauß and Leibnitz rules.

The term Γ_k represents the transfer of mass across the interface due to phase change

$$\Gamma_k \equiv \overline{\rho_k\left(\mathbf{v}_{k\mathrm{i}} - \mathbf{v}_{\mathrm{i}}\right) \cdot \nabla X_k}^V$$

where, due to the conservation of mass, the terms Γ_1 and Γ_2 satisfy the jump condition

$$\Gamma_1 + \Gamma_2 = 0$$

Here, as we do not consider phase change, we have from the kinematic boundary condition (19) the condition that the velocity at the interface is continuous. Thus, it is $\mathbf{v}_{1\mathrm{i}} = \mathbf{v}_{2\mathrm{i}} = \mathbf{v}_{\mathrm{i}}$ and we have $\Gamma_1 = \Gamma_2 = 0$.

The term $\mathbf{M}_k$ represents the momentum transfer across the interface

$$\mathbf{M}_k = -\overline{(-p_k \mathbb{I} + \mathbb{T}_k) \cdot \nabla X_k}^V \tag{32}$$

The sum of $\mathbf{M}_1$ and $\mathbf{M}_2$ satisfies the jump condition

$$\mathbf{M}_1 + \mathbf{M}_2 = \frac{1}{V} \int_{S_{\mathrm{i}} \cap V} \left(2H\sigma \hat{\mathbf{n}}_1 + \nabla_{\mathrm{s}} \sigma\right) \mathrm{d}S \tag{33}$$

which follows from volume averaging of the dynamic boundary condition (20). In the sequel we will assume that the coefficient of surface tension, σ, is constant, so that the second term under the integral is zero. While the equations (28) and (29) are valid in Ω_k only, the field equations (30) and (31) are valid in the entire domain Ω.

The motion of the interface or turbulence may introduce velocity fluctuations in each fluid. We account for the local spatial deviations from the volume averaged mean value by introducing for each phase the fluctuating velocity field

$$\mathbf{v}_k^{'} \equiv \mathbf{v}_k - \overline{\mathbf{v}_k}^k$$

Due to the non-linear convective term, this decomposition gives rise to a sub-grid stress (sgs) term in the volume averaged momentum equation (31), namely

$$\alpha_k \rho_k \overline{\mathbf{v}_k \mathbf{v}_k}^k = \alpha_k \rho_k \overline{\mathbf{v}_k}^k \overline{\mathbf{v}_k}^k - \alpha_k \mathbb{T}_k^{\mathrm{sgs}} \tag{34}$$

where

$$-\mathbb{T}_k^{\mathrm{sgs}} \equiv \underbrace{\rho_k\left(\overline{\overline{\mathbf{v}_k}^k \overline{\mathbf{v}_k}^k}^k - \overline{\mathbf{v}_k}^k \overline{\mathbf{v}_k}^k\right)}_{\mathbb{L}_k} + \underbrace{\rho_k\left(\overline{\overline{\mathbf{v}_k}^k \mathbf{v}_k^{'}}^k + \overline{\mathbf{v}_k^{'} \overline{\mathbf{v}_k}^k}^k\right)}_{\mathbb{C}_k} + \underbrace{\rho_k \overline{\mathbf{v}_k^{'} \mathbf{v}_k^{'}}^k}_{\mathbb{R}_k}$$

The tensors $\mathbb{L}_k$, $\mathbb{C}_k$, $\mathbb{R}_k$ represent the Leonard term, the cross term and the subgrid-scale Reynolds stress term, respectively. We note that in the case of time-averaging the subgrid-scale stresses are replaced by the respective turbulent stress tensor.

In this section we thus have obtained a set of two scalar and two vector equations representing the conservation of mass and momentum of the two phases. By applying the volume averaging operator to Eq. (24) we obtain a condition for the sum of the volume fractions

$$\alpha_1 + \alpha_2 = 1 \tag{35}$$

The set of equations derived here is unclosed, see section 3.3, and therefore model assumptions have to be introduced.

3.2.2 Volume averaged equations for two-phase mixture

The equations presented in section 3.2.1 describe the behavior of the individual phases. One can obtain equations describing the behavior of the two-phase mixture by summing up the equations of the individual phases. By summing up Eq. (30) for $k = 1$ and $k = 2$ we obtain for the mass conservation of the two-phase mixture the result

$$\sum_{k=1}^{2} \left[\frac{\partial \left(\alpha_k \rho_k \right)}{\partial t} + \nabla \cdot \alpha_k \rho_k \overline{\mathbf{v}_k}^k \right] = 0 \tag{36}$$

Defining a mixture density

$$\rho_\mathrm{m} \equiv \alpha_1 \rho_1 + \alpha_2 \rho_2 \tag{37}$$

and a center-of-mass velocity

$$\mathbf{v}_\mathrm{m} \equiv \frac{1}{\rho_\mathrm{m}} \sum_{k=1}^{2} \alpha_k \rho_k \overline{\mathbf{v}_k}^k = \frac{\alpha_1 \rho_1 \overline{\mathbf{v}_1}^1 + \alpha_2 \rho_2 \overline{\mathbf{v}_2}^2}{\alpha_1 \rho_1 + \alpha_2 \rho_2} \tag{38}$$

and introducing these definitions into Eq. (36) reduces it to the compact form

$$\frac{\partial \rho_\mathrm{m}}{\partial t} + \nabla \cdot \rho_\mathrm{m} \mathbf{v}_\mathrm{m} = 0 \tag{39}$$

This equation has the same form as for single-phase flow but the single-phase density and velocity are replaced by the mixture density and the center-of-mass velocity, respectively.

Summing up the volume averaged momentum equations (31) for both phases and introducing the jump condition (33) yields after some manipulations the following form for the **volume-averaged single-field momentum equation**

$$\begin{aligned} \frac{\partial \left(\rho_\mathrm{m} \mathbf{v}_\mathrm{m} \right)}{\partial t} \quad + \quad & \nabla \cdot \left(\rho_\mathrm{m} \mathbf{v}_\mathrm{m} \mathbf{v}_\mathrm{m} + \mathbb{D}_\mathrm{i} \right) = -\nabla \sum_{k=1}^{2} \alpha_k \overline{p_k}^k + \rho_\mathrm{m} \mathbf{g} + \frac{1}{V} \int_{S_\mathrm{i} \cap V} 2H\sigma \hat{\mathbf{n}}_1 \mathrm{d}S \\ & + \nabla \cdot \underbrace{\mu_\mathrm{m} \left(\nabla \mathbf{v}_\mathrm{m} + \left(\nabla \mathbf{v}_\mathrm{m} \right)^\mathrm{T} \right)}_{\mathbb{T}_\mathrm{m}} + \nabla \cdot \mathbb{T}_\mathrm{i} + \nabla \cdot \underbrace{\left(\alpha_1 \mathbb{T}_1^\mathrm{sgs} + \alpha_2 \mathbb{T}_2^\mathrm{sgs} \right)}_{\mathbb{T}_\mathrm{m}^\mathrm{sgs}} \end{aligned} \tag{40}$$

To explain the different terms in Eq. (40) we first introduce the relative velocity

$$\mathbf{v}_\mathrm{r} = \mathbf{v}_{21} \equiv \overline{\mathbf{v}_2}^2 - \overline{\mathbf{v}_1}^1 \tag{41}$$

which provides a measure of the mean velocity difference between the phases within the averaging volume V.

The term $\mathbb{D}_\mathrm{i}$ is the momentum drift-flux tensor

$$\mathbb{D}_\mathrm{i} \equiv \frac{\alpha_1\rho_1\alpha_2\rho_2}{\rho_\mathrm{m}}\mathbf{v}_\mathrm{r}\mathbf{v}_\mathrm{r} \tag{42}$$

It expresses the difference between the total resolved momentum flux and the flux of the averaged momentum due to the center-of-mass velocity. The definition of the interfacial friction tensor $\mathbb{T}_\mathrm{i}$ which arises from viscous forces is

$$\mathbb{T}_\mathrm{i} \equiv \rho_1\alpha_2\mu_2\left(\nabla\frac{\alpha_1\mathbf{v}_\mathrm{r}}{\rho_\mathrm{m}} + \left(\nabla\frac{\alpha_1\mathbf{v}_\mathrm{r}}{\rho_\mathrm{m}}\right)^\mathrm{T}\right) - \rho_2\alpha_1\mu_1\left(\nabla\frac{\alpha_2\mathbf{v}_\mathrm{r}}{\rho_\mathrm{m}} + \left(\nabla\frac{\alpha_2\mathbf{v}_\mathrm{r}}{\rho_\mathrm{m}}\right)^\mathrm{T}\right) \tag{43}$$

Note that the elements of the tensors $\mathbb{D}_\mathrm{i}$ and $\mathbb{T}_\mathrm{i}$ differ from zero only at respectively close to the interface.

3.3 Closure problem

In the previous section we obtained from the mass and momentum conservation of the phases eight scalar partial differential equations. In addition we have the algebraic constraint of Eq. (35) for the volume fractions and the three momentum jump conditions (one for each coordinate direction). We assume that the density and viscosity of each phase as well as the coefficient of surface tension are known. Then we have 12 scalar equations for in total 28 scalar unknowns. These unknowns are, for each phase, the volume fraction α_k, the three velocity components $\overline{\mathbf{v}_k}^k$, the pressure $\overline{p_k}^k$, the three components of the momentum transfer term $\mathbf{M}_k$, and the six components of the subgrid-scale stress tensor $\mathbb{T}_k^\mathrm{sgs}$.

For the remaining part of this section we will neglect the subgrid-scale stresses, i.e. we assume that

$$\mathbb{T}_1^\mathrm{sgs} = \mathbb{T}_2^\mathrm{sgs} = \mathbb{T}_\mathrm{m}^\mathrm{sgs} = 0 \tag{44}$$

so that there are only 16 unknowns left. One assumption which is very common in the modelling of two-phase flow by the continuous field or interpenetrating field approach is that both phases share the same pressure field, i.e.

$$\overline{p_1}^1 = \overline{p_2}^2 = p_\mathrm{m} \tag{45}$$

This reduces the number of unknowns to 15. Thus, three additional equations are needed to close the system of equations. The following sections presents three different concepts for these three closure relations.

3.4 Homogeneous model

3.4.1 Mathematical formulation

The homogeneous model is the most simple model within the continuous fields approach. It assumes that the phases move with the same velocity so that

$$\overline{\mathbf{v}_2}^2 = \overline{\mathbf{v}_1}^1 \tag{46}$$

Loosely spoken, the phases or fluids are in so called *mechanical equilibrium*. It follows by definition (41) that in this case the relative velocity is zero

$$\mathbf{v}_\mathrm{r} = 0 \tag{47}$$

Equation (46) respectively Eq. (47) provides the three additional scalar equations needed to close the system of equations. In the homogeneous model, therefore, only one velocity field needs to be computed. Because of Eq. (46) it is $\overline{\mathbf{v}_1}^1 = \overline{\mathbf{v}_2}^2 = \mathbf{v}_\mathrm{m}$. Thus, the velocity field is

obtained by solving the single-field Navier-Stokes equation (40) for the center-of-mass velocity. Because the relative velocity $\mathbf{v}_\mathrm{r}$ vanishes, so do the components of the tensors $\mathbb{D}_\mathrm{i}$ and $\mathbb{T}_\mathrm{i}$. With assumptions (44) and (45) the equations of the homogeneous model are then given by

$$\frac{\partial\left(\alpha_1\rho_1\right)}{\partial t} + \nabla\cdot\alpha_1\rho_1\mathbf{v}_\mathrm{m} = 0 \tag{48}$$

$$\frac{\partial\left(\alpha_2\rho_2\right)}{\partial t} + \nabla\cdot\alpha_2\rho_2\mathbf{v}_\mathrm{m} = 0 \tag{49}$$

$$\begin{aligned}\frac{\partial\left(\rho_\mathrm{m}\mathbf{v}_\mathrm{m}\right)}{\partial t} + \nabla\cdot\rho_\mathrm{m}\mathbf{v}_\mathrm{m}\mathbf{v}_\mathrm{m} &= -\nabla p_\mathrm{m} + \rho_\mathrm{m}\mathbf{g} + \nabla\cdot\mu_\mathrm{m}\left(\nabla\mathbf{v}_\mathrm{m} + \left(\nabla\mathbf{v}_\mathrm{m}\right)^\mathrm{T}\right) \\ &\quad + \frac{1}{V}\int_{S_\mathrm{i}\cap V} 2H\sigma\hat{\mathbf{n}}_1\mathrm{d}S\end{aligned} \tag{50}$$

We note that instead of Eq. (48) or Eq. (49) the conservation equation of the two-phase mixture, Eq. (39), can be used.

When the disperse fluid particle is fully inside the averaging volume V so that the interface does not cut the boundary ∂V of the averaging volume V, then the integral over the surface tension term drops out from Eq. (50) and the interface-momentum-transfer terms all cancel out. In this case, the momentum equation (50) is essentially a single phase transport equation, with variable density and viscosity.

From computational point of view, the assumption of the homogeneous model that the two phases share the same velocity field is a reasonable one under two remarkably distinct situations. The first one refers to finely dispersed flow, while the second corresponds to flows were the phases are well separated. We note that the distinction between dispersed and separated phases is mainly a matter of the length scale down to which one wants to resolve the flow, i.e. a matter of the size of the averaging volume. This length scale of averaging is itself usually related to the grid size chosen in a computation. Originally, the homogeneous model was developed for finely dispersed flow where the particle size is much smaller than the averaging volume and the size of a mesh cell. With the tremendous increase of computer power, however, nowadays huge number of grid points and fine meshes can be realized so that the homogenous model can be applied to separate flow as well.

3.4.2 Application to separate flow

An example for the application of the homogeneous model to separate flow is given by flows under strong influence of gravity such as stratified or wavy flow in a horizontal duct. In this case, the volume fractions of the phases are equal to one or zero everywhere except at the interface. In this situation it is meaningful to use a single velocity field. Because the interface is well resolved by the grid it will intersect the averaging volume V for some mesh cells. Therefore, the surface tension force needs to be considered in principle. However, within the homogeneous model it is usually neglected. We will discuss the modelling of surface tension in section 5.

3.4.3 Application to disperse flow

We now discuss the case of disperse flow. We suppose that the densities of the dispersed and continuous phases do differ. Then the phases tend to move with different velocity mainly due to two forces which involve the density (see Table 1). These are the buoyancy respectively gravitational force and the inertial force. On the other hand, the viscous force (viscous drag) tends to slow down the relative motion and will, in absence of a driving force, ultimately diminish it. Thus, the homogeneous model can be used when the interface momentum transfer is very large

so that the viscous forces (viscous drag) dominate over the buoyancy and inertia forces. For a fluid particle, the ratio between inertia forces and viscous forces is given by the particle Reynolds number, see section 2.4. Thus, from acceleration affects and in absence of gravity/buoyancy the application of the homogeneous model seems justified for particle Reynolds numbers less than unity.

Let us now consider the movement of a single particle within a stagnant liquid due to buoyancy. The ratio between the buoyancy force and the viscous force is given by

$$\frac{f_B}{f_V} = \frac{\Delta\rho g d_{\mathrm{eq}}^2}{\mu_{\mathrm{c}} V_{\mathrm{T}}} = \frac{EoRe}{We} = \sqrt{\frac{Eo^3}{MoRe^2}} = \frac{3}{4} Re\, C_{\mathrm{D}} \tag{51}$$

Introducing the Stokes drag law, Eq. (14), in Eq. (51) one obtains

$$\frac{f_B}{f_V} = 18$$

Thus, for the buoyancy driven motion of a fluid particle the ratio of buoyancy forces to viscous forces is always much larger than unity. This is to be expected because otherwise the particle would not move. This result suggests that for a dispersed flow where the particles movement is solely to the action of gravity/buoyancy the homogeneous model is not applicable. This is because bubbles rising or rigid particles falling in a surrounding stagnant liquid will quickly attain a fixed relative velocity where the drag force is in balance with the buoyancy and gravity force, see section 2.7.3. Due to this relative velocity the phase velocities are not equal and the homogeneous model can not be used. A more appropriate model for buoyancy driven dispersed flows is the diffusion model to be presented in the next section.

To summarize, for a disperse flow the assumption of homogeneous flow can be erroneous when a body force or acceleration field causes significant relative velocity or "slip" between the phases. Unless the drag force is very large a given pressure gradient will accelerate the gas far more rapidly than the liquid and cause a violation of the homogenous flow assumption. As a rule of thumb, the homogeneous model can be used for disperse flow to describe mixtures or suspensions of very small particles with diameter of say $d_{\mathrm{p}} < 0.1$ mm. Note, that the assumption of mechanical equilibrium made in the homogeneous model still allows the phase concentrations in the flow field to vary in space and time.

3.5 Diffusion model and drift-flux model

The diffusion model and drift-flux model can be considered as generalizations of the homogenous model. Both models do not assume that the phases are in mechanical equilibrium. So the phase velocities are allowed to differ from each other and consequently also differ from the mixture velocity. The main assumption of the diffusion model and the drift-flux model is that the relative velocity between the phases can be approximated by an algebraic expression.

In the **diffusion model** Eq. (47) is replaced by a *constitutive equation for the relative velocity*

$$\mathbf{v}_{\mathrm{r}} = \mathbf{v}_{\mathrm{r}}(\rho_1, \rho_2, \mu_1, \mu_2, \sigma, \alpha_1, \mathbf{v}_1, ...) \tag{52}$$

Beside this relation, the equations constituting the diffusion model are given by the mixture continuity equation (39), the mixture momentum equation (40) and the continuity equation for the gas phase

$$\frac{\partial\left(\alpha_2\rho_2\right)}{\partial t} + \nabla\cdot\alpha_2\rho_2\mathbf{v}_{\mathrm{m}} = -\nabla\cdot\alpha_1\alpha_2\frac{\rho_1\rho_2}{\rho_{\mathrm{m}}}\mathbf{v}_{\mathrm{r}} \tag{53}$$

From the r.h.s of Eq. (53) it can be seen that the relative velocity plays a role similar to that of the diffusion coefficient in a single-phase two-component system. This is where the model obtained its name from.

An example for the use of the diffusion model is given by Sokolichin & Eigenberger [31] who compute the bubble driven motion in a flat rectangular bubble column. The constitutive equation for the relative velocity is given by $\mathbf{v}_\mathrm{r} = (0,\ 0,\ 20\ \mathrm{cm/s})^\mathrm{T}$ where the third component corresponds to the vertical direction. The authors perform 2D and 3D laminar and turbulent simulations, using different kinds of discretization schemes on different grids. They find that only 3D turbulent simulations give grid-independent results that well agree with experiments, where an unsteady undulating bubble swarm is observed.

A variant of the diffusion model is the **drift-flux model**. The drift-flux model bears its name from the common practice to provide a constitutive equation not for $\mathbf{v}_\mathrm{r}$ but, instead, for the drift velocity of the disperse phase. The concept of the drift velocity was introduced by Zuber & Findley [40]. The drift-flux velocity of a phase is the velocity of the phase relative to the velocity of the volume-center of the mixture, given by

$$\mathbf{j}_\mathrm{m} \equiv \underbrace{\alpha_1 \overline{\mathbf{v}_1}^1}_{\mathbf{j}_1} + \underbrace{\alpha_2 \overline{\mathbf{v}_2}^2}_{\mathbf{j}_2} \tag{54}$$

The quantities $\mathbf{j}_1$ and $\mathbf{j}_2$ represent the volumetric flux densities of the continuous and disperse phase respectively, and $\mathbf{j}_\mathrm{m}$ is the volumetric flux density of the mixture. The velocities $\mathbf{j}_1$ and $\mathbf{j}_2$ are also called the superficial velocities of the continuous and disperse phase respectively, and $\mathbf{j}_\mathrm{m}$ is the total superficial velocity. Thus, the drift velocity of continuous and disperse phase are given by

$$\mathbf{v}_{1\mathrm{j}} \equiv \overline{\mathbf{v}_1}^1 - \mathbf{j}_\mathrm{m}, \quad \mathbf{v}_{2\mathrm{j}} \equiv \overline{\mathbf{v}_2}^2 - \mathbf{j}_\mathrm{m} \tag{55}$$

The phase drift velocities are related to the relative velocity via expressions

$$\mathbf{v}_{1\mathrm{j}} = -\alpha_2 \mathbf{v}_\mathrm{r}, \quad \mathbf{v}_{2\mathrm{j}} = \alpha_1 \mathbf{v}_\mathrm{r} \tag{56}$$

To close the drift-flux model, a constitutive equation for one of the drift velocities is required. Usually the closure relation is provided for the drift velocity of the disperse phase, i.e. for $\mathbf{v}_{2\mathrm{j}}$. The use of the drift-flux model is appropriate when the motions of the two phases are strongly coupled. Therefore, certain two-phase flow problems involving a sudden acceleration of one phase may not be appropriately described by the drift-flux model.

The drift-flux model is usually applied in its one-dimensional form. This is obtained by averaging the three-dimensional drift-flux model (obtained from time-averaging) over the cross-sectional area of the channel. However, the information on changes of variables in the direction normal to the flow is lost by this procedure. Appropriate closure relations for the one-dimensional drift-flux model were derived by Ishii [16] for various flow regimes and by Chexal & Lellouche [7] for vertical flows.

3.6 Two-fluid model or Euler-Euler model

3.6.1 The standard two-fluid model

The mathematical basis of the two-fluid model is given by the volume-averaged mass conservation equation (30) and momentum conservation equation (31) for each phase, or by the time-averaged counterparts of these equations, respectively. The momentum equations are coupled through the jump condition (33) for the transfer terms $\mathbf{M}_1$ and $\mathbf{M}_2$. In the two-fluid model the three scalar equations needed to close the set of equations are provided by a constitutive equation either for $\mathbf{M}_1$ or $\mathbf{M}_2$.

The definition of $\mathbf{M}_k$ is given by Eq. (32) which is repeated here for convenience

$$\mathbf{M}_k = -\overline{(-p_k\mathbb{I} + \mathbb{T}_k)\cdot\nabla X_k}^V = -\frac{1}{V}\int_V (-p_k\mathbb{I} + 2\mu_k\mathbb{D}_k)\cdot\nabla X_k \mathrm{d}V$$

Recalling that the gradient of the phase indicator function is related to the Dirac delta function of the interface, see Eq. (25), we can write

$$\mathbf{M}_k = -\frac{1}{V}\int_{S_\mathrm{i}\cap V}(-p_k\mathbb{I} + 2\mu_k\mathbb{D}_k)\cdot\hat{\mathbf{n}}_k \mathrm{d}S \tag{57}$$

So what is needed to close the two-fluid model is a constitutive equation for the integral of the instantaneous pressure and viscous stress distribution over the interface within the averaging volume V. Obviously, equation (57) is closely related to the force $\mathbf{F}_\mathrm{surf}$ exerted by the surrounding fluid on a particle, as expressed by Eq. (5). An important difference is that the integral in Eq. (5) is closed, i.e. is over the entire surface area $\mathcal{A}_\mathrm{p}$ of the particle, while the integral in Eq. (57) concerns only that part of the interfacial surface that is within the averaging volume V.

In section 2.6 the pressure was split in its static and dynamic components. Due to this splitting the force $\mathbf{F}_\mathrm{surf}$ was represented as the sum of three contributions, namely the buoyancy force, the force due to a linear pressure gradient, and the hydrodynamic force $\mathbf{F}_\mathrm{hydr}$. Here, we follow a similar approach and split the pressure of phase k into a mean interfacial pressure and a fluctuating pressure

$$p_k \equiv \overline{p_k}^{S_\mathrm{i}} + p_k'$$

The mean interfacial pressure is given by

$$\overline{p_k}^{S_\mathrm{i}} \equiv \frac{\displaystyle\int_{S_\mathrm{i}\cap V} p_k \mathrm{d}S}{\displaystyle\int_{S_\mathrm{i}\cap V}\mathrm{d}S} = \frac{1}{A_\mathrm{i}}\int_{S_\mathrm{i}\cap V} p_k \mathrm{d}S \tag{58}$$

where A_i is the area of $S_\mathrm{i}\cap V$. Introducing the interfacial area concentration

$$a_\mathrm{i} \equiv \frac{A_\mathrm{i}}{V} = \frac{1}{V}\int_{S_\mathrm{i}\cap V}\mathrm{d}S = \frac{1}{V}\int_V \delta(\mathbf{x}-\mathbf{x}_\mathrm{i})\mathrm{d}V = \frac{1}{V}\int_V \hat{\mathbf{n}}_k\cdot\hat{\mathbf{n}}_k\delta(\mathbf{x}-\mathbf{x}_\mathrm{i})\mathrm{d}V = \overline{\hat{\mathbf{n}}_k\cdot\nabla X_k}^V$$

equation (58) can be written as

$$\overline{p_k}^{S_\mathrm{i}} \equiv \frac{1}{A_\mathrm{i}}\int_{S_\mathrm{i}\cap V} p_k \mathrm{d}S = \frac{\overline{p_k\hat{\mathbf{n}}_k\cdot\nabla X_k}^V}{\overline{\hat{\mathbf{n}}_k\cdot\nabla X_k}^V}$$

Introducing the splitting of Eq. (58) in Eq. (32) we obtain

$$\mathbf{M}_k = \overline{\overline{p_k}^{S_\mathrm{i}}\mathbb{I}\cdot\nabla X_k}^V \underbrace{-\overline{\left(-p_k'\mathbb{I}+\mathbb{T}_k\right)\cdot\nabla X_k}^V}_{\mathbf{M}_{k,\mathrm{h}}} = \overline{p_k}^{S_\mathrm{i}}\overline{\nabla X_k}^V + \mathbf{M}_{k,\mathrm{h}} = \overline{p_k}^{S_\mathrm{i}}\nabla\alpha_k + \mathbf{M}_{k,\mathrm{h}} \tag{59}$$

The term $\overline{p_k}^{S_\mathrm{i}}\nabla\alpha_k$ then contains the force contributions due to a hydrostatic pressure gradient and any external pressure gradient. It gives a net contribution only in case when there are any gradients of the volume fraction. On the other hand, the term $\mathbf{M}_{k,\mathrm{h}}$ includes only hydrodynamic contributions and thus is non-zero only if there exists a relative motion between the phases.

Inserting Eqs. (59) and Eq. (34) in Eq. (31), taking advantage of the product rule

$$\nabla\left(\alpha_k\overline{p_k}^k\right) = \alpha_k\nabla\overline{p_k}^k + \overline{p_k}^k\nabla\alpha_k$$

and assuming that the interfacial-area averaged pressure is equal to the volume averaged pressure

$$\overline{p_k}^{S_\mathrm{i}} \approx \overline{p_k}^k \tag{60}$$

we obtain the momentum equation for the two phases in the form

$$\frac{\partial\left(\alpha_k\rho_k\overline{\mathbf{v}_k}^k\right)}{\partial t}+\nabla\cdot\alpha_k\rho_k\overline{\mathbf{v}_k}^k\overline{\mathbf{v}_k}^k=-\alpha_k\nabla\overline{p_k}^k+\alpha_k\rho_k\mathbf{g}+\nabla\cdot\alpha_k\overline{\mathbb{T}_k}^k+\nabla\cdot\alpha_k\mathbb{T}_k^{\mathrm{sgs}}+\mathbf{M}_{k,\mathrm{h}}$$

Introducing Eq. (59) in the momentum jump condition (33) and using assumption (60) the jump condition for the hydrodynamic momentum transfer terms becomes

$$\mathbf{M}_{1,\mathrm{h}}+\mathbf{M}_{2,\mathrm{h}}=\frac{1}{V}\int_{S_\mathrm{i}\cap V}\left(2H\sigma\hat{\mathbf{n}}_1+\nabla_\mathrm{s}\sigma\right)\mathrm{d}S \tag{61}$$

To close the two-fluid model a constitutive equation for one of the two hydrodynamic momentum transfer terms is still needed. Here, we provide closures for the term $\mathbf{M}_{1,\mathrm{h}}$. Because this term involves the fluctuating pressure p_k' and the viscous stresses at the interface we expect that it will strongly depend on the flow regime. In this paper we will derive closure relations only for the case of dispersed two-phase flows.

In the two-fluid model it is commonly assumed that the typical volume $\mathcal{V}_\mathrm{p}$ of a disperse particle is much smaller then the averaging volume V. Then, neglecting that particles may intersect the border ∂V of the averaging volume, the term $\mathbf{M}_{1,\mathrm{h}}$ can be approximated as

$$\begin{aligned}\mathbf{M}_{1,\mathrm{h}} &= -\frac{1}{V}\int_{S_\mathrm{i}\cap V}\left(-p_1'\mathbb{I}+2\mu_1\mathbb{D}_1\right)\cdot\hat{\mathbf{n}}_1\mathrm{d}S\approx-\frac{1}{V}\sum_{j=1}^{N_\mathrm{p}}\oint_{\mathcal{A}_\mathrm{p}^j}\left(-p_1'\mathbb{I}+2\mu_1\mathbb{D}_1\right)\cdot\hat{\mathbf{n}}_1\mathrm{d}S\\ &= -\frac{1}{V}\sum_{j=1}^{N_\mathrm{p}}\mathbf{F}_{\mathrm{hydr}}^j\end{aligned} \tag{62}$$

where N_p is the number of particles within V and $\mathcal{A}_\mathrm{p}^j$ denotes the interfacial area of particle j. The jump condition (61) then becomes

$$\mathbf{M}_{1,\mathrm{h}}+\mathbf{M}_{2,\mathrm{h}}=\frac{1}{V}\sum_{j=1}^{N_\mathrm{p}}\oint_{\mathcal{A}_\mathrm{p}^j}\left(2H\sigma\hat{\mathbf{n}}_1+\nabla_\mathrm{s}\sigma\right)\mathrm{d}S=0$$

An important assumption of the two-fluid model is, therefore, that the (up to now arbitrary) volume V over which the phasic averaging is performed must be considerable larger than the characteristic length scale of the dispersed phase (e.g. the particle diameter) and much smaller than the characteristic macroscopic (geometrical) length scale of the flow problem. In practice, however, the averaging volume is usually not explicitly specified.

When all particles within V have the same size, i.e. the flow is locally mono-disperse, each particle will experience the same force and equation (62) can be simplified to

$$\mathbf{M}_{1,\mathrm{h}}=-\frac{N_\mathrm{p}}{V}\,\mathbf{F}_{\mathrm{hydr}}=-n_\mathrm{p}\,\mathbf{F}_{\mathrm{hydr}} \tag{63}$$

Here, n_p is the local number density i.e. the local number of particles per unit volume. This quantity is an unknown. What is known from the solution of the disperse phase mass conservation equation is the local volumetric fraction α_2 of the disperse phase. From α_2 the local number density can be computed only when an assumption on the particle volume respectively the equivalent diameter d_eq is made

$$n_\mathrm{p}=\frac{N_\mathrm{p}}{V}=\frac{N_\mathrm{p}\mathcal{V}_\mathrm{p}}{V}\frac{1}{\mathcal{V}_\mathrm{p}}=\frac{\alpha_2}{\mathcal{V}_\mathrm{p}}=\frac{6\alpha_2}{\pi d_\mathrm{eq}^3} \tag{64}$$

While in equation (64) in principle d_{eq} is a *local* equivalent diameter, in the standard two-fluid model a *global* equivalent diameter is adopted. Thus, it is assumed that the flow is mono-disperse in the entire computational domain, so that d_{eq} is constant in space and time. The specification of the equivalent diameter is probably the most important closure assumption introduced in the two-fluid model. This assumption is appropriate for mono-disperse rigid particles but needs careful consideration for flows with bubbles or droplets.

In section 2.6 it was mentioned that the hydrodynamic force $\mathbf{F}_{\mathrm{hydr}}$ is usually represented as the sum of several contributions, namely the drag force, the added mass force, the history force, and the lift force, see Eq. (9). Therefore Eq. (63) becomes

$$\mathbf{M}_{1,\mathrm{h}} = -\frac{\alpha_2}{\mathcal{V}_{\mathrm{p}}} \left(\mathbf{F}_{\mathrm{drag}} + \mathbf{F}_{\mathrm{am}} + \mathbf{F}_{\mathrm{lift}} + \mathbf{F}_{\mathrm{hist}} \right) \equiv \mathbf{M}_{1,\mathrm{drag}} + \mathbf{M}_{1,\mathrm{am}} + \mathbf{M}_{1,\mathrm{lift}} + \mathbf{M}_{1,\mathrm{hist}} \tag{65}$$

while the jump conditions are

$$\mathbf{M}_{2,\mathrm{drag}} = -\mathbf{M}_{1,\mathrm{drag}}, \quad \mathbf{M}_{2,\mathrm{am}} = -\mathbf{M}_{1,\mathrm{am}}, \quad \mathbf{M}_{2,\mathrm{lift}} = -\mathbf{M}_{1,\mathrm{lift}}, \quad \mathbf{M}_{2,\mathrm{hist}} = -\mathbf{M}_{1,\mathrm{hist}}$$

To close the two-fluid model the forces in Eq. (65) must be modelled. Depending on the actual flow under investigation some of these forces may be neglected. A force that can be neglected under most circumstances und thus will not be considered here is the history force.

The most important one of the hydrodynamic forces is the **drag force**. In the two-fluid model the drag force is modelled in analogy to Eq. (12) and is given by

$$\mathbf{F}_{\mathrm{drag}} = -\frac{1}{2} C_{\mathrm{D}} \rho_1 \mathcal{A}_{\mathrm{pcs}} |\overline{\mathbf{v}_2}^2 - \overline{\mathbf{v}_1}^1| \left(\overline{\mathbf{v}_2}^2 - \overline{\mathbf{v}_1}^1 \right)$$

Thus, in the two-fluid model the characteristic relative velocity $\mathbf{U}_{\mathrm{r}}$ from Eq. (10) is represented as $\overline{\mathbf{v}_2}^2 - \overline{\mathbf{v}_1}^1$. The particle velocity $\mathbf{V}_{\mathrm{p}}$ is thus approximated by $\overline{\mathbf{v}_2}^2$ while the characteristic velocity of the continuous phase $\mathbf{U}_{\mathrm{c}}$ is taken as $\overline{\mathbf{v}_1}^1$. Both velocities $\overline{\mathbf{v}_1}^1$ and $\overline{\mathbf{v}_2}^2$ are field quantities and defined in the entire computational domain. In the two-fluid model the particle Reynolds number defined in Eq. (13) thus becomes

$$Re_{\mathrm{p}} = \frac{\rho_1 d_{\mathrm{eq}} |\overline{\mathbf{v}_2}^2 - \overline{\mathbf{v}_1}^1|}{\mu_1}$$

Expressions that relate the drag coefficient of an isolated rigid particle to the particle Reynolds number were already discussed in section 2.6. For rigid particles in a dilute flow a drag law that combines the Schiller-Naumannn correlation (15) with the constant value of Newton's regime is often used

$$C_{\mathrm{D}}(Re_{\mathrm{p}}) = \begin{cases} \dfrac{24}{Re_{\mathrm{p}}} \left(1 + 0.15 Re_{\mathrm{p}}^{0.687} \right) & \text{for } 0 \leq Re_{\mathrm{p}} < 1.000 \\ 0.44 & \text{for } 1.000 \leq Re_{\mathrm{p}} < 3.5 \cdot 10^5 \end{cases}$$

For dilute bubbly flow Tomiyama et al. [35] proposed drag laws that take into account the contamination of the continuous phase. The drag law for a pure system is given by

$$C_{\mathrm{D}} = \max \left\{ \min \left[\frac{16}{Re} \left(1 + 0.15 Re_p^{0.687} \right), \frac{48}{Re} \right], \frac{8}{3} \frac{Eo}{Eo + 4} \right\}$$

that for a slightly contaminated system by

$$C_{\mathrm{D}} = \max \left\{ \min \left[\frac{24}{Re} \left(1 + 0.15 Re_p^{0.687} \right), \frac{72}{Re} \right], \frac{8}{3} \frac{Eo}{Eo + 4} \right\}$$

and that for a fully contaminated system by

$$C_{\mathrm{D}} = \max\left\{ \frac{48}{Re}\left(1 + 0.15 Re_p^{0.687}\right), \frac{8}{3}\frac{Eo}{Eo+4} \right\}$$

The drag-correlations given above are appropriate as long as the flow can be considered as dilute, i.e. the local disperse phase volume fraction is below say 0.1 % everywhere. Hydrodynamic constitutive relations for closure of the two-fluid model for non-dilute flows are given by Ishii & Mishima [18] for solid particles, bubbles and drops for the complete range of void fractions and will not be listed here.

The model commonly employed for the **added mass force** is given by

$$\mathbf{F}_{\mathrm{am}} = C_{\mathrm{am}} \rho_1 \mathcal{V}_{\mathrm{p}} \left(\frac{\mathrm{D}_2 \overline{\mathbf{v}_2}^2}{\mathrm{D}t} - \frac{\mathrm{D}_1 \overline{\mathbf{v}_1}^1}{\mathrm{D}t} \right)$$

where

$$\frac{\mathrm{D}_k}{\mathrm{D}t} \equiv \frac{\partial}{\partial t} + \overline{\mathbf{v}_k}^k \cdot \nabla$$

For an isolated spherical particle within an infinite fluid the value of the added mass coefficient is $C_{\mathrm{am}} = 1/2$. For multiple bubbles C_{am} slightly increases with the volume fraction of the disperse phase

$$C_{\mathrm{am}} = \frac{1}{2} + \frac{K}{2}\alpha_2 \quad \text{where} \quad K \approx 3$$

For the **lift force** several models have been proposed in literature. Here, we give only one model for the shear-induced lift force [4, 11]

$$\mathbf{F}_{\mathrm{lift}} = -C_{\mathrm{lift}} \rho_1 \mathcal{V}_{\mathrm{p}} \left(\overline{\mathbf{v}_2}^2 - \overline{\mathbf{v}_1}^1 \right) \times \nabla \times \overline{\mathbf{v}_1}^1$$

The lift coefficient C_{lift} is a function not only of the particle Reynolds number but also of the shear Reynolds number of the continuous phase flow. For bubbles C_{lift} is a function of the Eötvös number, too. For large values of the Eötvös number (i.e. large deformable bubbles) the wake-induced lift force becomes dominant over the shear-induced lift force. Then, for upward flow, the effective lift force is not directed towards the walls but to the channel center [36].

A weakness of the common lift force model is that it results in a wall-directed force on the particle even very close to the wall. In a simulation this may result in the non-physical situation that the void fraction takes a local maximum at the wall while in reality the void fraction at the wall is zero for a bubbly flow. To circumvent this problem a wall force or **wall lubrication force** is introduced in [3]. This force acts normal to the wall and points in the center of the channel. It is non-zero only very close to the wall and counterbalances the lift force so that a physically reasonable decrease of the void fraction in close vicinity of the wall is ensured. A physical argument for the wall lubrication force is that the centroid of a spherical bubble of given diameter can not approach closer to the wall than half of the bubbles diameter.

3.6.2 Closure relations for non-disperse two-phase flow

While disperse flows are of special interest for chemical and nuclear engineering there exists, as shown in Figure 1 and 2, a number of other flow regimes where the phases flow separately. In the oil industry for example flow regimes typical for pipelines such as stratified flow, wavy flow and slug flow are of special interest. It is obvious that for these flow regimes the closure assumptions of disperse flows given above can not be used. Issa & Kempf [20] performed simulations of slug flow in horizontal and nearly horizontal pipes with a one-dimensional transient two-fluid model. For this purpose the authors developed a model for the frictional forces between the phases at the interface.

3.6.3 Well-posedness of the two-fluid model

A specific topic related to the mathematical formulation of the two-fluid model is that of "well-posedness". In order for a problem involving a partial differential equation to be well-posed, the solution to the problem must exist and be unique, and the solution must depend continuously upon the initial or boundary data [1].

Well-posedness is a property of the modelling process, rather than a specific property of the flow itself and requires that the model appropriately reflects the physics of the flow. A necessary condition for an initial-value problem to be well-posed is that the governing differential equations should possess real characteristics. For incompressible flow the two-fluid model has been shown to possess real characteristics when the relative velocity between the two phases falls below a certain value. For a discussion on the well-posedness of the one-dimensional two-fluid model see e.g. [34].

3.7 Modern extensions of the two-fluid model

With the conventional two-fluid model for disperse flows presented above in a strict sense only globally mono-disperse flows or flows with a globally constant number density can be computed. In a real disperse two-phase flow, however, often a spectrum of bubble sizes is present. If breakup or coalescence occurs, neither the bubble diameter nor the number density are spatially uniform or constant in time. To overcome these restrictions the two-fluid model must be conceptually extended. In the following we will discuss three different concepts that are actually under development.

3.7.1 Transport equation for interfacial area concentration

The first approach, introduced in [17], is based on the intuition that in a two-phase flow not only the volumetric concentration of the phases is important, but also the interfacial area concentration. The available interfacial area influences not only the viscous and form drag but is also of special relevance when heat or mass transfer processes take place at the interface. The interfacial area concentration can be defined based on statistical averaging, time averaging and volume averaging, see [26]. Here, we consider the volumetric interfacial area concentration a_i, i.e. the interfacial area per unit volume, which is for a disperse flow given by

$$a_\mathrm{i} = \frac{1}{V}\sum_{j=1}^{N_\mathrm{p}} \mathcal{A}_\mathrm{p}^j$$

For a mono-disperse system the above equation simplifies to $a_\mathrm{i} = n_\mathrm{p}\mathcal{A}_\mathrm{p}$. In this case the number density is related with the interfacial area concentration, void fraction, and sphericity ψ (see Eq. (2)) via expression

$$n_\mathrm{p} = \frac{\psi^3}{36\pi}\frac{a_\mathrm{i}^3}{\alpha_2^2} \tag{66}$$

Hence, when the sphericity ψ is known or assumed and the interfacial area concentration is known, too, Eq. (66) can replace Eq. (64). We emphasize that a benefit of Eq. (66) over Eq. (64) is only achieved when the interfacial area concentration is a local quantity. This then corresponds to a local equivalent diameter by means of relation

$$d_\mathrm{eq} = \frac{6}{\psi}\frac{\alpha_2}{a_\mathrm{i}}$$

Thus, the assumption of a *global* mono-disperse flow in the standard two-fluid model is replaced by the assumption of a *local* mono-disperse flow.

Ishii [15] proposed to solve a scalar transport equation to determine local values for a_i. With α_2 and a_i given, for a locally mono-disperse flow with spherical bubbles the local number density $n_\mathrm{p}(\mathbf{x}, t)$ respectively the local equivalent diameter can be computed. Thus, the solution of a transport equation for the interfacial area concentration has the advantage that now the bubble diameter needed for the specification of the interfacial transfer terms is no more a global but a local quantity.

The interfacial area transport equation can be derived by considering the fluid particle number density equation analogous to Boltzmann's transport equation [22]. It has the form

$$\frac{\partial a_\mathrm{i}}{\partial t} + \nabla \cdot (a_\mathrm{i} \mathbf{v}_{a_\mathrm{i}}) = \Phi_{a_\mathrm{i}} \tag{67}$$

Here, $\mathbf{v}_{a_\mathrm{i}}$ is the transport velocity of the volumetric interfacial area and Φ_{a_i} a source term taking into account the different phenomena creating or destroying interfacial area, such as coalescence or breakup of bubbles or droplets, phase change or interfacial stretching. Morel et al. [26] showed that Eq. (67) can be derived without assuming any particular geometrical configuration of the interfaces, so that Eq. (67) can be applied independently of the flow regime.

The major problem in development of the transport equation for the interfacial area concentration is that of formulating adequate models for the source/sink term Φ_{a_i} [19]. It has been demonstrated that the one-dimensional interfacial area transport equation can give a good prediction for bubbly flows in vertical tubes with tube diameters in the range 25–50 mm [13].

Even if the standard two-fluid model is extended by a transport equation for the interfacial area equation a distinct disadvantage is that the sphericity of the bubble still needs to be specified, see Eq. (66). Therefore, with one transport equation for the interfacial area concentration a change of the particle size can be modelled but not a change of the particle shape. To overcome this disadvantage recently the concept of two-group interfacial area transport has been proposed by Ishii et al. [19] as a more general approach. In this approach the bubbles are treated in two groups and for each group a separate transport equation for the interfacial area concentration is solved. The first group represents spherical and distorted (e.g. ellipsoidal) bubbles while the second group represents cap-type bubbles and elongated bubbles typical for slug flow. It is hoped that this approach can replace the traditional flow regime maps and regime transition criteria that do not dynamically represent the changes in the interfacial structure. Instead, the changes in the two-phase flow structure are predicted mechanistically by introducing the interfacial area transport equation for two groups.

3.7.2 Population balance equations

Another promising concept to overcome the mono-disperse flow limitation of the standard two-fluid model flow is based on the introduction of population classes. In this approach the disperse phase is divided in N classes. Each class covers its own range of bubble diameters and is treated as a separate field. For each class a mass balance equation and a momentum equation is solved leading in total to $N + 1$ coupled continuity equations and $N + 1$ momentum equations. Depending on N this approach can consume extensive computer resources. Here, no mathematical details will be given.

Models for breakup and coalescence suitable for the population balance approach can for example be found in [38]. In that paper 2D simulations for an aerated stirred vessel are presented where $N = 25$ bubble classes are taken into account. The simulations are, however, not based on the two-fluid model. Instead it is assumed that the gas bubbles do not significantly alter the flow field. Therefore, a steady liquid flow field is computed by a single-phase simulation.

To limit the computational costs of the population balance approach Lo [25] proposed the so-called Multiple Size Group (MUSIG) model. MUSIG assumes that all the velocities of the

different particle classes can be algebraically related to the average velocity of the disperse phase. Therefore, only one momentum equation is solved for the disperse phase. However, the N continuity equations of the particle classes are retained and solved to represent the size distribution.

The main advantage of the interfacial area concentration transport equation or population balance equations over the two-fluid model is that bubble-bubble interactions are explicitly taken into account. With the population balance equations even local bubble size distributions can be computed. This offers the possibility of investigating the internal gas-liquid structure and can be used to improve e.g. the computation of mass-transfer processes.

3.7.3 Four-field two-fluid model

The four-field two-fluid-model developed by Lahey and Drew [23] can be considered as an extension of the two-fluid model. It considers two fluids or phases, which are denoted here as "liquid" and "vapor". The basic idea is that each phase may be continuous in some regions of space while it is dispersed in some other regions of space. Typical examples are given by the slug flow and annular flow regimes illustrated in Figure 1. In the four-field two-fluid model the four fields are therefore given by continuous liquid (cl), continuous vapor (cv), disperse liquid (dl) and disperse vapor (dv). For each of these four fields separate transport equations for mass and momentum are solved. Similar to the two-fluid model these equations are coupled by mass and momentum transfer terms which must be modelled. Closure relations and results for various types of two-phase flows are given in [23]. The four field two fluid model seems to be very promising especially for flows where phase change phenomena such as boiling or condensation do occur.

4 Euler-Lagrange method

4.1 Conceptual approach of the Euler-Lagrange method

The two-fluid model presented in section 3.6 can in principle be used to compute any two-phase flow regime, supposed an adequate closure relation for the momentum transfer term is provided. In this section we present the Euler-Lagrange method that it suitable only for disperse flows. The method bears its name from the fact that the continuous phase is treated in an Eulerian manner, while the disperse phase is treated in a Lagrangian manner. In the Eulerian approach the flow variables are a function of space and time and thus are represented as fields. In the Lagrangian approach instead individual particles are considered and the position and velocity of each particle is a function of time only. In the Euler-Lagrange approach therefore a mass and momentum conservation equation is solved for the continuous phase, similar to the two-fluid model. For the disperse phase, in contrast, the position and velocity of each particle is obtained from Newton's second law. This requires the interpolation of the continuous phase velocity from the Eulerian grid to the local particle position.

For flows involving a (comparatively) small number of dispersed particles it is possible to solve a set of Lagrangian equations for every element. However, if the number of particles is large, a statistical approach is more practical. Then, the total population is represented by a finite number of computational parcels (samples), each of which represents a group (cluster) of particles having the same properties. The Euler-Lagrange method may, however, face problems whenever the cloud of particles tracked is larger than the fluid parcel over which volume averaging is performed. Also, the number of samples is not arbitrary, but must be large enough so that the properties of the full population are well represented. This can be assessed, in the absence of any other measures, by performing calculations with different numbers of samples and comparing

the results. In a Euler-Lagrange computation typically 10,000 – 100,000 particles or parcels are considered.

4.2 Coupling between phases

The Euler-Lagrange method can be classified with respect to the kind of coupling between the phases. The simplest approach is that of **one-way coupling**. In a one-way coupled system the particle mass-loading respectively volume-loading is assumed to be small enough so that any effects that the presence of the dispersed phase may have on the continuous phase can be neglected. Thus, the local velocity of the continuous phase has a direct impact on the particle motion while the reverse is not true. If the effects of the particles on the carrier fluid can not be ignored **two-way coupling** is required. So called **four-way coupling** additionally takes into account the particle-particle collision effects due to higher void fraction of the dispersed phase and due to turbulence modification by particles. The state of the art of the method can be found in [8]. A rough estimate which kind of coupling is appropriate can be obtained from the volume fraction of the disperse phase. For very low values, say $\alpha_\mathrm{p} < 10^{-6}$, one-way coupling can be used while two way coupling may be a reasonable approach up to $\alpha_\mathrm{p} \approx 10^{-3}$. For higher values four-way coupling should be used [32].

In this paper only one-way coupling is considered. One way coupling has the significant advantage that the Eulerian velocity field can be computed independent of the particle tracking by a standard single-phase simulation. For a steady flow for example, the continuous phase velocity field can be obtained once at the beginning. The trajectories of the individual particles can then be computed independently from one another. This makes the one-way coupled Euler-Lagrange method ideally suited for parallel computers. In contrast, a two-way coupled Euler-Lagrange simulation must in general be done in an iterative manner or fully time-dependent. In four-way coupling the particles interact e.g. by collisions. These can be modelled directly by tracking all particles simultaneously, or by a statistical approach based on the generation of fictitious collisions partner, see e.g. [33]. In confined flows such as in pneumatic transport or in cyclones used for particle separation it is important to model wall collisions of the particles. Here, we will not discuss this topic, but refer to textbook [8].

4.3 Particle equation of motion

We now give the equation describing the translational motion of a particle. This equation needs to be solved in the Lagrange part of the Euler-Lagrange method. We denote the position vector to the center-of-mass of the particle by $\mathbf{X}_\mathrm{p}(t)$. Then the translational velocity of the center-of-mass of the particle is given by

$$\mathbf{V}_\mathrm{p}(t) = \frac{\mathrm{d}\mathbf{X}_\mathrm{p}(t)}{\mathrm{d}t}$$

The translational motion of the particle is governed by Newton's second law

$$\frac{\mathrm{d}}{\mathrm{d}t}\left(m_\mathrm{p}\mathbf{V}_\mathrm{p}\right) = \mathbf{F}_\mathrm{surf} + \mathbf{F}_\mathrm{body}$$

Here, $m_\mathrm{p} = \rho_\mathrm{d}\mathcal{V}_\mathrm{p}$ is the mass of the particle. In the sequel we assume that the density $\rho_\mathrm{p} = \rho_\mathrm{d} = \rho_2$ and the particle volume $\mathcal{V}_\mathrm{p}$ are constant in time and so is the particle mass. $\mathbf{F}_\mathrm{surf}$ is the resulting force exerted on the particles surface as given in Eq. (7) and $\mathbf{F}_\mathrm{body}$ is the body force. Here we assume that the only body force is due to gravity

$$\mathbf{F}_\mathrm{body} = \rho_\mathrm{p}\mathbf{g}$$

Then we obtain

$$\rho_\mathrm{p}\mathcal{V}_\mathrm{p}\frac{\mathrm{d}\mathbf{V}_\mathrm{p}}{\mathrm{d}t} = \mathbf{F}_\mathrm{surf} + \mathbf{F}_\mathrm{body} = \mathcal{V}_\mathrm{p}\left(\rho_\mathrm{p} - \rho_1\right)\mathbf{g} - \mathcal{V}_\mathrm{p}P_\mathrm{pg}\hat{\mathbf{e}}_\mathrm{p} + \mathbf{F}_\mathrm{hydr}$$

Introducing the split of the hydrodynamic force from Eq. (9) we have:

$$\rho_\mathrm{p}\mathcal{V}_\mathrm{p}\frac{\mathrm{d}\mathbf{V}_\mathrm{p}}{\mathrm{d}t} = \mathcal{V}_\mathrm{p}\left(\rho_\mathrm{p} - \rho_1\right)\mathbf{g} - \mathcal{V}_\mathrm{p}P_\mathrm{pg}\hat{\mathbf{e}}_\mathrm{p} + \mathbf{F}_\mathrm{drag} + \mathbf{F}_\mathrm{am} + \mathbf{F}_\mathrm{hist} + \mathbf{F}_\mathrm{lift} \tag{68}$$

For the hydrodynamic forces the models introduced in section 3.6.1 for the closure of the two-fluid model can be used when $\overline{\mathbf{v}_2}^2$ is replaced by $\mathbf{V}_\mathrm{p}$. Thus, in the Euler-Lagrange method in the definition of the relative velocity $\mathbf{U}_\mathrm{r}$ the particle velocity $\mathbf{V}_\mathrm{p}$ is retained, while the characteristic velocity of the continuous phase is set to $\mathbf{U}_\mathrm{c} = \overline{\mathbf{v}_1}^1(\mathbf{X}_\mathrm{p}(t))$.

For non-spherical rigid particles the particle rotation may become important. This requires that in addition to the translation equation of motion the angular momentum equation for each particle needs to be solved. This topic is not discussed here.

4.4 Particle response time and Stokes number

A useful concept for a simple characterization of the motion of a particle is that of the particle response time. To explain this quantity we consider a simplified equation of motion where only the inertia force and the drag force are present

$$\rho_\mathrm{p}\mathcal{V}_\mathrm{p}\frac{\mathrm{d}\mathbf{V}_\mathrm{p}}{\mathrm{d}t} = \mathbf{F}_\mathrm{drag} = -\frac{1}{2}C_\mathrm{D}\rho_1\mathcal{A}_\mathrm{pcs}\left(\mathbf{V}_\mathrm{p} - \overline{\mathbf{v}_1}^1\right)\left|\mathbf{V}_\mathrm{p} - \overline{\mathbf{v}_1}^1\right| \tag{69}$$

With $\mathcal{A}_\mathrm{pcs} \approx \pi d_\mathrm{eq}^2/4$ and

$$Re_\mathrm{p} = \frac{\rho_1 d_\mathrm{eq}|\mathbf{V}_\mathrm{p} - \overline{\mathbf{v}_1}^1|}{\mu_1}$$

equation (69) can be written as

$$\frac{\mathrm{d}\mathbf{V}_\mathrm{p}}{\mathrm{d}t} = \frac{3}{4}\frac{\mu_1}{\rho_\mathrm{p}d_\mathrm{eq}^2}C_\mathrm{D}Re_\mathrm{p}\left(\overline{\mathbf{v}_1}^1 - \mathbf{V}_\mathrm{p}\right) \tag{70}$$

The term $(3/4)(\mu_1/\rho_\mathrm{p}d_\mathrm{eq}^2)C_\mathrm{D}Re_\mathrm{p}$ has the dimension of a frequency (s^{-1}). The invers of this term has, therefore, the dimension of a time and is called the **particle response time**

$$\tau_\mathrm{p} \equiv \frac{4}{3}\frac{\rho_\mathrm{p}d_\mathrm{eq}^2}{\mu_1}\frac{1}{C_\mathrm{D}Re_\mathrm{p}} \tag{71}$$

Introducing the latter definition in the simplified equation of motion (69) reduces it to the instructive form

$$\frac{\mathrm{d}\mathbf{V}_\mathrm{p}}{\mathrm{d}t} = \frac{\overline{\mathbf{v}_1}^1 - \mathbf{V}_\mathrm{p}}{\tau_\mathrm{p}}$$

We thus see that for $\overline{\mathbf{v}_1}^1 > \mathbf{V}_\mathrm{p}$ the particle velocity $\mathbf{V}_\mathrm{p}$ increases, for $\overline{\mathbf{v}_1}^1 < \mathbf{V}_\mathrm{p}$ the particle velocity $\mathbf{V}_\mathrm{p}$ decreases while for $\overline{\mathbf{v}_1}^1 = \mathbf{V}_\mathrm{p}$ the particle velocity $\mathbf{V}_\mathrm{p}$ does not change in time.

For interpretation of the particle response time we give a simple one-dimensional example. We consider the motion of a particle initially at rest within a surrounding fluid flowing with uniform velocity U_∞. The last equation then becomes

$$\frac{\mathrm{d}V_\mathrm{p}}{\mathrm{d}t} = \frac{U_\infty - V_\mathrm{p}}{\tau_\mathrm{p}}$$

The solution of this equation for the initial condition $V_\mathrm{p}(0) = 0$ is given by

$$V_\mathrm{p}(t) = U_\infty \left(1 - \exp\left(-t/\tau_\mathrm{p}\right)\right)$$

For $t = \tau_\mathrm{p}$ we thus obtain

$$\frac{V_\mathrm{p}(\tau_\mathrm{p})}{U_\infty} = 1 - e^{-1} \approx 0.632$$

Thus the particle response time is the time the particle needs to accelerate from rest to 63 % of the continuous phase velocity. More generally, the particle response time can be interpreted as the characteristic time the particle needs to respond (or answer) to a sudden change of the fluid velocity.

For Stokes flow with $C_\mathrm{D} = 24/Re_\mathrm{p}$ the particle response time becomes

$$\tau_\mathrm{p,St} = \frac{\rho_\mathrm{p} d_\mathrm{p}^2}{18\mu_1}$$

The particle response time constitutes a characteristic time scale for changes of the particle velocity. Similarly we can define a characteristic time scale for velocity changes in the continuous phase (carrier phase). A characteristic time sale for the macroscopic motion of the carrier phase is given by

$$\tau_\mathrm{c,macro} \equiv \frac{L}{U_\mathrm{c}}$$

where L is a characteristic dimension of the channel, e.g. the hydraulic diameter of the channel, and U_c is a characteristic velocity, e.g. the mean axial velocity.

For a turbulent flow a characteristic time scale for the turbulent velocity fluctuations of the carrier phase is

$$\tau_\mathrm{c,turb} \equiv \frac{k}{\varepsilon}$$

where k is the turbulent kinetic energy and ε its dissipation rate.

A characteristic time scale for the smallest eddies in the carrier flow is given by the Kolmogorov time scale

$$\tau_\mathrm{c,K} \equiv \sqrt{\frac{\mu_\mathrm{c}}{\rho_\mathrm{c}\varepsilon}}$$

The ratio of the particle response time to a time scale of the carrier phase motion defines the **Stokes number**. For example, the Stokes number computed with the Kolmogorov time scale is given by

$$St_\mathrm{K} \equiv \frac{\tau_\mathrm{p}}{\tau_\mathrm{c,K}}$$

There are two limiting cases for St_K. For $St_\mathrm{K} \to 0$ the particle completely follows the motion of the carrier phase while for $St_\mathrm{K} \to \infty$ the motion of the particle and of the carrier phase are totally uncorrelated. In practice both situations do hardly occur. Instead, the particle will answer with a certain delay on local velocity changes of the carrier phase.

4.5 Turbulent dispersion

A conceptual difficulty arises when the flow of the carrier phase is turbulent. In this case often a turbulence model such as the popular $k - \varepsilon$ model is employed[1]. By this approach only the time mean value of the continuous phase velocity field is computed as well as the time mean value of the turbulent kinetic energy k. A single particle is, however, transported by the local

[1] For an introduction to turbulence modeling see e.g. textbook [12]

instantaneous turbulent velocity field but not by the time-averaged mean velocity field. Due to the fluctuating character of the turbulent velocity field macroscopically a dispersion of particles released nominally at the the same position is observed. This effect is called *turbulent dispersion* and is absent in any Euler-Lagrange computation where only the mean velocity field is taken into account. A common approach to model the turbulent dispersion is to represent the carrier velocity field as sum of the known local time averaged velocity and a fluctuation

$$\mathbf{v}_1(\mathbf{x},t) = \overline{\mathbf{v}_1}^t(\mathbf{x}) + \mathbf{v}_1'(\mathbf{x},t)$$

The fluctuation is often modelled in a stochastic manner by assuming a Gaussian probability function with zero mean value and a standard deviation given by $\sqrt{2k/3}$.

The above procedure is valid for a one-way coupled system. However, for a non-zero Stokes number the particle does not fully follow the instantaneous turbulent fluid motion due to its inertia. Moreover, the velocity non-equilibrium characteristic for large particles will enable these particles to interact with several turbulent eddies which reduces the particle's residence time in each eddy and mitigates the influence of the eddy on the particle trajectory [8]. This effect is called the *crossing trajectory effect*.

5 Interface resolving methods (direct numerical simulation)

In this section we consider the flow of two fluid phases, i.e. gas-liquid and liquid-liquid flow. For these flows the diffusion model, the two-fluid model and the Euler-Lagrange model do all require a priori information on the flow regime. For the dispersed flow regime, for example, the standard models require a priori knowledge of the shape of the bubbles or drops. The standard two-fluid model even requires knowledge on the size of the bubble or drop. In contrast, the interface resolving simulation or direct numerical simulation aims to describe in detail the deformation and topological evolution of the phase-interface separating the two fluids. Physically, the deformation of the phase-interface is intimately connected with the surface tension force. Therefore, any method for direct numerical simulation of gas-liquid or liquid-liquid flow relies on a reliable representation of the surface tension force.

The main difficulty of interface resolving simulations is the moving interface whose shape is part of the solution. In addition, physical quantities such as density, viscosity and pressure are discontinuous across the interface. Mathematically, the interface is treated as a surface of discontinuity. Loosely spoken it is "sharp". To keep the interface numerically sharp, i.e. to avoid any artificial smearing of the interface during the computation, special numerical methods have been developed. Nowadays mainly three methods are used. The volume-of-fluid method (VOF) [14] is the oldest one while the level-set method [30] and the front-tracking method [37] have been developed in the last decade. All these methods are formulated for incompressible fluids only and solve only one single momentum equation.

5.1 Volume-of-fluid method

The basic idea of the VOF method [14] is the definition of a scalar quantity f which represents the fraction of the volume of a mesh cell occupied by one phase, say the liquid (phase 1). Thus, for $f = 1$ the mesh cell is entirely filled with liquid, while for $f = 0$ it is entirely filled with gas. In a mesh cell that instantaneously contains a part of the interface both phases coexist and $0 < f < 1$.

The set of equations of the volume-of-fluid method is in principle equivalent with the set of equations of the homogeneous model, see Eqs. (48 – 50). However, it is assumed that the averaging volume V is identical with the mesh cell volume V_c. Thus we have $\alpha_1 = f$ and $\alpha_2 = 1 - f$. It is further assumed that the mesh cell is so small that (i) the interface curvature is

well resolved, (ii) the relative velocity in interface mesh cells is zero ($\mathbf{v}_\mathrm{r} = 0$) so that $\mathbb{D}_\mathrm{i} = \mathbb{T}_\mathrm{i} = 0$, and (iii) all scales of turbulence are resolved by the grid so that $\mathbb{T}_\mathrm{m}^\mathrm{sgs} = 0$.

The mass conservation of both phases is expressed by a transport equation for the liquid volumetric fraction f

$$\frac{\partial f}{\partial t} + \nabla \cdot f\mathbf{v}_\mathrm{m} = 0 \tag{72}$$

and by the condition of a divergence free velocity field

$$\nabla \cdot \mathbf{v}_\mathrm{m} = 0 \tag{73}$$

Under the assumption of constant densities ρ_1 and ρ_2 equation (72) follows from Eq. (48) by diving through ρ_1 while Eq. (73) can be obtained by division of Eq. (48) by ρ_1 and division of Eq. (49) by ρ_2 and summing up both equations.

As f has large gradients at the interface, Eq. (72) is not solved by standard difference schemes because this would result in numerical smearing of the interface. In the VOF method the f-equation is instead solved in a "geometrical" manner. For this purpose, by taking advantage of the Gauß divergence theorem, the convective term in Eq. (72) is written as a surface integral

$$\frac{\partial f}{\partial t} + \frac{1}{V_c} \oint_{\partial V_c} X_1 \mathbf{v}_1 \cdot \hat{\mathbf{n}}_{\partial V_c} \mathrm{d}S = 0 \tag{74}$$

where $\hat{\mathbf{n}}_{\partial V_c}$ is the unit normal vector of the boundary ∂V_c pointing outward of V_c. So what is needed to evaluate the above equation is the knowledge of the velocity $\mathbf{v}_1$ and the phase distribution at the faces of a mesh cell. The velocity $\mathbf{v}_1$ is obtained by solution of the momentum equation (50) and by assuming $\mathbf{v}_1 \approx \mathbf{v}_\mathrm{m}$. The phase distribution within a mesh cell is obtained by a reconstruction of the interface.

In general, there are two types of VOF reconstruction schemes. In SLIC methods (Simple Line Interface Calculation) the interface is assumed to be orientated parallel to the face of a mesh cell. In a 2D case the interface is therefore orientated either horizontally or vertically. The actual orientation depends on the values of f in neighboring mesh cells. In PLIC methods (Piecewise Linear Interface Calculation) the interface is represented in 2D by a line and in 3D by a plane. The orientation of the line or plane can be arbitrary. A plane is uniquely represented by a point within the plane and by its unit normal vector. For evaluation of the unit normal vector a large number of different reconstruction schemes exists in literature. In general, the unit normal vector is approximated as a discrete representation of relation

$$\hat{\mathbf{n}}_1 = \frac{\nabla f}{|\nabla f|}$$

A disadvantage of current PLIC methods is that the planes representing the interface in two neighboring mesh cells are not continuous at the mesh cell face that both mesh cells are sharing. Once the unit normal vector is computed the point within the plane can be computed by parallel shift of the plane within a mesh cell so that the liquid volume fraction in the cell just equals the value $f_{i,j,k}$ of the respective mesh cell.

After completion of the interface reconstruction step Eq. (74) can be solved by computing the liquid volume fluxes across all the mesh cell faces within a time step Δt. For this advection step two different approaches exist in literature. In *operator split methods* the reconstruction and advection is done for each coordinate direction separately. Thus, in 3D three consecutive reconstruction and advection steps are required per time step. In *unsplit methods* there is only one reconstruction step and the volume fluxes across the mesh cell faces are computed simultaneously. The disadvantage of the unsplit method is that the same liquid volume may be advected twice or even triply. Nevertheless, a key advantage of the volume-of-fluid method as

compared e.g. to the level-set and front-tracking method is its excellent conservation of mass of the two phases.

To compute the surface tension force the interface curvature must be computed. This can be done in analogy to Eq. (23):

$$\kappa = 2H = -\nabla \cdot \hat{\mathbf{n}}_1$$

As $\hat{\mathbf{n}}_1$ is constant in V_c and assuming σ to be constant, too, the surface tension term can be computed as

$$\frac{1}{V_c}\int_{S_\mathrm{i}\cap V_c} 2H\sigma\hat{\mathbf{n}}_1 \mathrm{d}S = \frac{\sigma}{V_c}\hat{\mathbf{n}}_1 \int_{S_\mathrm{i}\cap V_c} \kappa \,\mathrm{d}S = \frac{A_\mathrm{i}}{V_c}\sigma\hat{\mathbf{n}}_1\overline{\kappa}^{S_\mathrm{i}} = a_\mathrm{i}\sigma\hat{\mathbf{n}}_1\overline{\kappa}^{S_\mathrm{i}}$$

Here, a_i is the interfacial area concentration within the mesh cell and

$$\overline{\kappa}^{S_\mathrm{i}} \equiv \frac{1}{A_\mathrm{i}}\int_{S_\mathrm{i}\cap V_c} \kappa \,\mathrm{d}S$$

is the interfacial-area averaged curvature. From the reconstructed interface the area A_i can easily be determined.

5.2 Level-set method

The level-set method [30] follows a different approach to avoid smearing of the interface. The idea of the method is to define the interface as the zero level set of a *smooth* scalar function ϕ,

$$S_\mathrm{i} = \{\mathbf{x} \mid \phi(\mathbf{x}, t) = 0\}$$

In the gas region (region with fluid 2) it is taken $\phi < 0$ and in the liquid region (region with fluid 1) $\phi > 0$. Therefore one has

$$\phi(\mathbf{x}, t) = \begin{cases} > 0 & \text{if } \mathbf{x} \in \text{phase 1} \\ = 0 & \text{if } \mathbf{x} \in S_\mathrm{i} \\ < 0 & \text{if } \mathbf{x} \in \text{phase 2} \end{cases}$$

In practice, ϕ is usually taken as the signed distance from the interface. The phase distribution is then computed by solving the advection equation

$$\frac{\partial \phi}{\partial t} + \nabla \cdot \phi\mathbf{v} = 0$$

Since ϕ is a smooth function this equation can be solved by standard finite difference schemes.

The level-set method is based on a fully local single-field formulation of the momentum equation. So there is no volume averaging of the governing equations. In the level-set method the surface tension term is given by

$$\mathbf{F}_\sigma = \int_{\partial A_\mathrm{i}} \sigma\kappa\delta(\mathbf{x} - \mathbf{x}_\mathrm{i})\hat{\mathbf{n}}_1 \mathrm{d}S$$

The unit normal on the interface pointing into fluid 1 and the curvature of the interface can easily be expressed in terms of $\phi(\mathbf{x}, t)$:

$$\hat{\mathbf{n}}_1 = \left.\frac{\nabla\phi}{|\nabla\phi|}\right|_{\phi=0} \quad \text{and} \quad \kappa = -\nabla \cdot \left.\left(\frac{\nabla\phi}{|\nabla\phi|}\right)\right|_{\phi=0}$$

For representation of the Dirac delta function at the interface several proposals exist in literature.

Advantages of the level-set method are that, unlike in the VOF method, the interface is represented as a continuous surface. Furthermore, there is no need for complex interface reconstruction. Phenomena such as breakup or coalescence can be treated in a rather simple manner. Disadvantages of the method are that the signed distance function ϕ must be re-initialized after each time step and the method does not exactly conserve mass.

5.3 Front-tracking method

The front-tracking method was developed by Tryggvason and coworkers [37]. Similar to the level-set method the front-tracking method is based on a local single-field formulation of the momentum equation which is discretized by finite differences. The key idea of the method is to compute the velocity field from the solution of the momentum equation on a fixed regular grid, while the phase interface is represented by a set of marker particles. These marker particles are advected with the local velocity, which is interpolated from the fixed grid to the position of the marker particles. After the particle advection step is completed the phase interface is newly structured and marker particles are added or removed to ensure a locally adequate resolution of the phase interface. In a next step, the surface tension is computed using polynomial fits and is then interpolated from the front grid to the fixed grid. Also the density and viscosity field are updated to the new interface position. To avoid discontinuities, the surface tension force as well as the density and viscosity are smoothed over two to three mesh cells. Then, the velocity field for the next time step is computed from the single-field momentum equation.

Advantages of the front-tracking method are the accurate representation of the interface as continuous surface. A disadvantage is that topological changes of the interface such as break-up and coalescence are difficult to handle and require additional measures. Nevertheless, the front-tracking method is a very powerful method and 3D simulations involving up to 256 bubbles have been performed.

Acknowledgement

The author is grateful to Prof. E. Mamut, organizer of the "International Summer School on Computational Modeling of Combustion & Multiphase Flows in Energy Systems", for providing the opportunity to give this lecture. Additional thanks go to B. Ghidersa, M. Ilić and W. Sengpiel for carefully reading the manuscript.

References

[1] D.A. Anderson, J.C. Tannehill and R.H. Pletcher, *Computational Fluid Mechanics and Heat Transfer*, Hemisphere Publishing Co., 1984.

[2] D.M. Anderson, G.B. McFadden and A.A. Wheeler, Diffuse-interface methods in fluid mechanics, Annu. Rev. Fluid Mech. **30** (1998) 139-165.

[3] S.P. Antal, R.T. Lahey and J.E. Flaherty, Analyis of phase distribution in fully developed laminar bubbly two-phase flow, Int. J. Multiphase Flow **17** (1991) 635–652.

[4] T.R. Auton, The lift force on a spherical body in a rotational flow, J. Fluid Mech. **183** (1987) 199–218.

[5] H.D. Baehr and K. Stephan, *Heat and mass transfer*, Springer Verlag, Berlin, 1998.

[6] A.B. Basset, *A treatise on Hydrodynamics*, Chapter 21, Dover Publications, New York, 1961.

[7] B. Chexal and G. Lellouche, A full-range drift-flux correlation for vertical flows (Revision 1), EPRI NP-3989-SR Special Report, September 1986.

[8] C. Crowe, M. Sommerfeld and Y. Tsuji, *Multiphase Flows with Droplets and Particles*, CRC Press, Boca Raton, 1998.

[9] R. Clift, J.R. Grace and M.E. Weber, *Bubbles, drops, and particles*, Academic Press, 1978.

[10] D.A. Drew and S.L. Passman, *Theory of Multicomponent Fluids*, Applied Mathematical Sciences, Volume 135, Springer, New York, 1999.

[11] D.A. Drew and R.T. Lahey, The virtual mass and lift force on a sphere in rotating and straining insviscid flow, Int. J. Multiphase Flow **13** (1987) 113–121.

[12] P.A. Durbin and B.A. Pettersson Reif, Statistical theory and modeling for turbulent flows, Wiley, Chichester, 2001.

[13] T. Hibiki and M. Ishii, Development of one-group interfacial area transport equation in bubbly flow systems, Int. J. Heat Mass Trans. **45** (2002) 2351-2372.

[14] C.W. Hirt and B.D. Nichols, Volume of Fluid (VoF) method for the dynamics of free boundaries, J. Comput. Phys. **39** (1981) 201–225.

[15] M. Ishii, *Thermo-Fluid Dynamic Theory of Two-Phase Flow*, Eyrolles, Paris, 1975.

[16] M. Ishii, One-dimensional drift-flux model and constitutive equations for relative motion between phases in various two-phase flow regimes, Argonne National Laboratory report ANL-77-47, 1977.

[17] M. Ishii and K. Mishima, Study of two-fluid model and interfacial area, Argonne National Laboratory report ANL-80-111, 1981.

[18] M. Ishii and K. Mishima, Two-fluid model and hydrodynamic constitutive relations, Nucl. Eng. Design **82** (1984) 107-126.

[19] M. Ishii, X. Sun and S. Kim, Modelling strategy of the source and sink terms in the two-group interfacial area transport equation, Ann. Nucl. Energy **30** (2003) 1309–1331.

[20] R.I. Issa and M.H.W. Kempf, Simulation of slug flow in horizontal and nearly horizontal pipes with the two-fluid model, Int. J. Multiphase Flow **29** (2003) 69–95.

[21] R. Jackson, *The dynamics of fluidized particles*, Cambridge University Press, 2000.

[22] G. Kocamustafaogullari and M. Ishii, Foundation of the interfacial area transport equation and its closure relations, Int. J. Heat Mass Trans. **38** (1995) 481-493.

[23] R.T. Lahey and D.A. Drew, The analysis of two-phase flow and heat transfer using a multidimensional, four field, two-fluid model, Nucl. Eng. Design **204** (2001) 29-41.

[24] V.G. Levich, *Physicochemical Hydrodynamics*, Prentice Hall, New York, 1962.

[25] S. Lo, Application of population balance to CFD modelling of bubbly flows via the MUSIG model, Proc. 4th Int. Conf. Gas-Liquid-Solid Reactor Engineering, Delft, August 23–25, 1999, pp. 1–8.

[26] C. Morel, N. Goreaud and J.-M. Delhaye, The local volumetric interfacial area transport equation: derivation and physical significance, Int. J. Multiphase Flow **25** (1999) 1099-1128.

[27] J.F. Richardson and W.N. Zaki, Sedimentation and fluidization, Trans. Inst. Chem. Engnrs. **32** (1955) 35-53.

[28] P.G. Saffman, The lift on a small sphere in a slow shear flow, J. Fluid Mech. **22** (1965) 385-400.

[29] P.G. Saffman, Corrigendum, J. Fluid Mech. **31** (1968) 624.

[30] J.A. Sethian, *Level set methods and fast marching methods : evolving interfaces in computational geometry, fluid mechanics, computer vision, and materials science*, Cambridge University Press, 1999.

[31] A. Sokolichin and G. Eigenberger, Applicability of the standard $k-\varepsilon$ turbulence model to the dynamic simulation of bubble columns: Part I. Detailed numerical simulations, Chem. Eng. Science **54** (1999) 2273-2284.

[32] M. Sommerfeld, Theoretical and experimental modelling of particulate flows - Overview and fundamentals, VKI Lecture Series 2000–06, 1–62.

[33] M. Sommerfeld, Validation of a stochastic Lagragian modelling approach for inter-particle collisions in homogeneous isotropic turbulence, Int. J. Multiphase Flow **27** (2001) 1829–1858.

[34] J.H. Song and M. Ishii, The well-posedness of incompressible one-dimensional two-fluid model, Int. J. Heat Mass Transf. **43** (2000) 2221-2231.

[35] A. Tomiyama, I. Kataoka, I. Zun and T. Sakaguchi, Drag coefficients of single bubbles under normal and micro gravity conditions, JSME Int. J. Series B **41** (1998) 472–479.

[36] A. Tomiyama, H. Tamai, I. Zun and S. Hosokawa, Transverse migration of single bubbles in simple shear flows, Chem. Eng. Science **57** (2002) 1849–1858.

[37] G. Tryggvason, B. Bunner, A. Esmaeli, D. Juric, N. Al-Rawahi, W. Tauber, J. Han, S. Nas and Y.-J. Jan, A front-tracking method for the computations of multiphase flow, J. Comput. Phys. **169** (2001) 708-759.

[38] B.C.H. Venneker, J.J. Derksen and H.E.A. van den Akker, Population balance modeling of aerated stirred vessels based on CFD, AIChE Journal **48** (2002) 673-685.

[39] S. Whitaker, *The Method of Volume averaging*, Kluwer Academic Publishers, Dordrecht, 1999.

[40] N. Zuber and J.A. Findlay, Average volumetric concentration in two-phase flow systems, J. Heat Transfer **87** (1965) 453-468.